ESTIMATION OF OPTIMUM DYNAMIC LAND USE PARAMETERS IN HYDROLOGIC MODELS USING REMOTELY SENSED DATA

A Thesis Submitted in Partial Fulfillment of the Requirements

for the Degree of

MASTER OF TECHNOLOGY

by

Sanjeev Kumar Jha

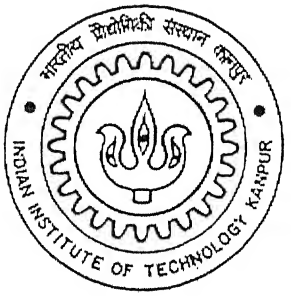

to the

DEPARTMENT OF CIVIL ENGINEERING
INDIAN INSTITUTE OF TECHNOLOGY, KANPUR

JULY, 2004

CERTIFICATE

This is to certify that the thesis entitled **"Estimation of Optimum Dynamic land use parameters in Hydrologic Models using Remotely Sensed Data,** by Sanjeev Kumar Jha, Roll No. Y3103044 has been carried out under my supervision in partial fulfillment of the requirements for the degree of Master of Technology in Civil Engineering at Indian Institute of Technology Kanpur, India.

Prof. Dr.-Ing. Manfred Ostrowski
Technical University Darmstadt,
Institute for Hydraulic Engineering
and Water Management,
Petersenstraße 13,
64287 Darmstadt,
Germany.

Dr. Ashu Jain
Department of Civil Engineering
Indian Institute of Technology, Kanpur
Kanpur – 208016
India

ACKNOWLDEGEMENT

I would like to express my deep sense of gratitude and profound thanks to *Professor Manfred W. Ostrowski*, for his keen interest and guidance. His constant encouragement and perseverance were constant sources of inspiration for me.

I am also greatly indebted to *Professor Ashu Jain* for his invaluable guidance, constant encouragement and inspiration throughout the course of this work.

I owe my sincere thanks to *Dipl.-Ing./M.Sc. Arne Klawitter* for giving me the confidence to work with WBM model and for his invaluable help for the successful completion of this project. I am also grateful to *Dr.-Ing. Detlev Belke* for providing the necessary inputs in terms of computer facility. Thanks are also due to all members of the Water Resources group from Department of Civil Engineering, TU-Darmstadt, for their cooperation and friendliness during my stay in Germany.

I also gratefully acknowledge the financial support from the German Academic Exchange Service (*DAAD*) during the course of this project in Germany. Further, I would like to take this opportunity to thank all my teachers for sharing their knowledge with me and also would like to specially thank all my friends for the moral support they provided.

With Thanks and Regards

Sanjeev Kumar Jha

Y3103044

SYNOPSIS

A spatial water balance model for the Tarrawarra catchment in Australia has been set up in order to investigate the effect of changes in dynamic land uses on water balance. Detailed Meteorological and runoff data, soil profiles, soil moisture patterns were available for this catchment. The data were processed to prepare the input files required to run the WBM model. The simulations were conducted using a 6 minute time step. The model parameters were set by a careful analysis of the available field data, with subsequent hydraulic conductivity parameters. The model performed reasonably well, although there was some tendency for the model to overestimate the surface runoff. This showed difficult and challenging task to simulate saturation excess runoff. Different calibration trials were attempted to achieve a best combination of model parameters for which there would be exact match in time series graphs. Finally a set of parameters were concluded based on time series graph and error statistics results.

Effect of introduction of different types of forests in the catchment showed logical results; which implied that the WBM model could be used for prediction of differences in water balance and suitably developing an urban area in the catchment. This will provide a direction to the city planners to conserve water resources by planting a definite amount of land for buildings and selection of appropriate types of trees to be planted.

CONTENTS

Chapter 7 – SUMMARY AND CONCLUSIONS

LIST OF FIGURES

LIST OF TABLES

Chapter 1

Introduction

1.1 General

Mathematical models of watershed hydrology are fundamental to water resources assessment, development and mangement. They are used to analyse the quantity and quality of streamflow, reservoir system operations, groundwater development and protection, surface water and groundwater conjuctive use management, water distribution systems, water use and a range of water resources management activities (Wurbs 1998). Watersheds may be modelled by a lumped model using basin average input data and producing total basin streamflow. Such a model may produce reasonable results but because of the distributed nature of hydrological properties like soil type, slope and land-use, the model cannot be expected to accurately represent the watershed conditions. Distributed hydrological models like TOPOG, Water balance model (WBM) provide an effective simulation tool for exploring basin hydrological processes and predicting the effects of change on catchment response. Distributed models preserve the spatial variability by dividing the model domain into small, interconnected cells, which makes them suitable for distributed hydrologic forecasting to better represent watershed features. The conjunctive use of distributed hydrologic models and field or remote observations

permit the comparison of spatial patterns in hydrology which ultimately increase our insight on the hydrological processes operating in a basin.

Modeling of the hydrologic system has been the subject of research among hydrologists and engineers for a very long time. The transformation of rainfall into runoff is an extremely complex, dynamic, and non-linear process which is affected by many factors which are often inter-related. The factors affecting the runoff response of a watershed subjected to rainfall input include (a) storm characteristics i.e. intensity and duration of rainfall event, (b) watershed characteristics i.e. size, shape, slope, and storage characteristics of the watershed, percent of the watershed contributing runoff at the outlet at various time steps during a rainfall event, etc., (c) geo – morphological characteristics of a watershed i.e. topography, land use patterns, vegetation, soil types, etc., that affect the infiltration, and (d) climatic characteristics such as temperature, humidity, wind characteristics, etc. The influence of these factors and many of their combinations in generating runoff is an extremely complex physical process and is not understood clearly (Zhang and Govindaraju, 2000). Many of the rainfall-runoff models rely on the fact that the dynamic effects of various factors mentioned above are embedded in the rainfall and runoff data.

Historically, Hydrologists and researchers have employed deterministic model or Conceptual model that considers the physics of the underlying process. These models use the equations of mass, energy, and momentum to describe the movement of water over land surface and through the unsaturated and saturated zones of the earth (Birikundavyi et

al., 2002). There are several hydrologic models developed by different organisations across the globe. There is no common agreement to accept any of the developed models as the standard one due to heterogeneous land use and unpredictable climatic conditions for the different catchment systems. The use of emerging technologies of Remote sensing and Geographical information system (GIS) has proven their usefulness in development of efficient hydrologic models.

1.2 Role of spatial data tools in hydrologic modeling

Many types of hydrological analysis are limited by a lack of spatial data, since traditionally hydrological data are point measurements. Remote sensing data are fundamentally different, they incorporate spatial information. The rapidly developing geographical information system (GIS) technology is a powerful tool to organize, process and visualize spatial data. The GIS technology can be usefully employed for data management, data retrieval, manipulations, organisations and the like - that may be entirely suitable for development of distributed models. Thus, remote sensing (RS) and GIS can complement each other and enable hydrological models to be more physically based and more efficient. It is only during the last five years that an integration of RS and GIS with hydrological models became technically feasible (Baumgartner et al 1997). GIS has provided a new environment to develop distributed hydrological models. These models take into account and predict the values of the studied phenomena at any point within the watershed (Mitas and Mitasova 1998). Zhang (1997) developed a framework integrating a stochastic space-time rainfall model and a distributed hydrologic simulation with GIS.

The remote sensing technology has many advantages (Schultz, 1988). It produces areal measurements in place of point measurements. All informations are collected and stored at one place. It offers high resolution in space and time. Data are available in digital form. Data acquisition does not interface with data observation. Data can be gathered for remote areas that are otherwise inaccessible. Once the remote sensing networks are installed, data measurements are relatively inexpensive.

Remote sensing data from Satellite are useful in watershed modelling in two ways. First, Satellite data can be used to better define soils and land covers over a watershed, which are needed to determine infiltration, evapotranspiration and runoff. Second, remote sensing measures data over space rather than at a point, and can, therefore be used to correct errors in input data based on point measurements as is with rainfall, evaporation. Using these techniques, it is possible to generate three dimensional watershed model, including precipitation, surface runoff, porous media flow, open channel flow, interaction of ground water and channel flow, and transport of water to the atmosphere by evaporation and transpiration.

The GIS can efficiently combination the different data such as topography, soil maps, rainfall distribution etc. The integrated use of satellite imagery and GIS technologies provide spatial and temporal input parameters to the models. Remote sensing permits the observation of data over large and inaccessible areas and monitoring of land use changes in a river basin. The effect of land use changes on hydrologic cycle can be understood by

estimating the sensitive parameters influencing the hydrological processes. Dynamic land use parameters can be thought of in terms of root depth, vegetation density, leaf area index, percentage of unproductive land i.e. urban areas, surface roughness, albedo and interception storage.

1.3 Objectives

The objective of this work can be summarised in four steps:

1) To understand the importance of conceptual hydrologic models;
2) Explore how to use the WBM model and incorporate RS data in simulating hydrological processes of a catchment;
3) Estimate the values of parameters of the WBM model;
4) Prediction of change in water balance due to dynamic land use changes in the catchment using calibrated WBM model.

1.4 Layout of the report

This report is specifically intended to give in detail description of using hydrologic modelling to observe the change in water balance due to dynamic land use. The presents chapter gives an overview of hydrologic modelling and role of RS and GIS in hydrologic modelling and presents the objective of the thesis. At the beginning, in second chapter, literature review has been presented. Third chapter discusses about the WBM model used in this study. Fourth chapter describes the catchment under study along with summary of

available data; preparation of input files required to run the model and selection of periods for calibration and validation of the model. Next chapter deals with estimation of model parameters using trial and error procedure. Chapter 6 discusses the sensitivity of dynamic land use parameters and its affect on water balance. The last chapter presents the conclusion of the study and scope for future study.

Chapter 2

Literature Review

2.1 General

Watershed hydrology is the branch of hydrology which deals with the infiltration of hydrologic processes at the watershed to determine the watershed response (Singh, 2002). The watershed may be as small as a parking lot or as a large as river basin. The quantitative description of the land phase of the hydrologic cycle is very complicated due to spatial non-uniformity defined by climate, topography, geology, soils, vegetation and land use. Watershed modelling is required for varied purposes such as water resources assessment like water quality evaluation, development like planning and designing soil conservation practices and management like irrigation water management. These models are utilized to quantify the impacts of watershed management strategies, linking human activities within the watershed to water quantity and quality of the receiving stream or lake for environmental and water resource protection. There is abundance of literature available in the area of hydrologic modelling using conceptual methods. This chapter reviews some of the important hydrologic models relevant to the present study.

In the early 1960's the Stanford Watershed Model (SWM) was instrumental in introducing the civil engineering profession to the concept of continuous hydrologic modeling.

Crawford and Linsley (1966) developed SWM to describe entire hydrologic cycle. SWM has undergone many revisions since its development initially. Some other popular models from the computer age are the watershed models of Dawdy and O´ Donnell (1965); HEC-1 (Hydrologic Engineering Center 1968); SWMM (Metcalf and Eddy et al. (1971); PRMS (Leavesley et al. 1983); NWS river forecast system (Burnash et al. 1973a,b); SSARR (Rockwood 1982); Systeme Hydrologique European (SHE) (Abbott et al. 1986a,b); TOPOMODEL (Beven and Kirkby 1979); and IHDM (Morris 1980). Most of these models use the laws of physics to simulate various components of the hydrologic cycle.

During the decades of 1970s and 1980s, with the digital revolution, a number of mathematical models were developed not only for simulation of watershed hydrology; but also for their applications in other areas, such as environmental and ecosystem management.

Singh (2002) has presented an overview of the hydrologic models used in different countries. HEC-HMS is considered as the standard model in the private sector in the United states for the design of drainage systems, quantifying the effect of land use change on flooding etc. The UBC and WATFLOOD models are popular in Canada for hydrologic simulation. The RORB and WBN models are commonly employed for flood forecasting, drainage design and evaluating the effect of land-use changes in Australia. TOPMODEL and SHE are the standard models for hydrologic analysis in many European countries. The HBV model is the standard model for flow forecasting in Scandinavian countries. The

ARNO, LCS and TOPIKAPI models are popular in Italy. The Tank models are well accepted in Japan. The Xinanjiang model is a commonly used model in China.

Most of the deterministic hydrologic models need a large amount data for calibration and validation purposes and are computationally extensive. The parameters of the model needs to be first calibrated before it can used for predicting runoff. Calibration of the model has been the subject of research among hydrologists. Normally, rainfall and runoff data for representative storms taken from a watershed under consideration are employed for this purpose. New technique of Genetic algorithms is becoming popular in finding the optimal parameters of a model. It is interesting to understand modelling concepts and interdependency between model parameters and error objective function surfaces, particularly when the model is used to determine the likely effects of land use changes. In this case, it requires to deal with spatial variability and scaling.

2.2 The major types of Hydrological models

Durand [2002] reported that most of the models used in hydrology fit into one of the following categories.

i. Black box empirical models (BBMs): The relationship between the input signal and the output signal is derived from long series of observations, using statistical time series analysis, multivariate regression or computing tools.

ii. Lumped conceptual models (LCMs): The catchment is considered as a whole, and the system is modelled using a conceptual, "metaphysical" vision, e.g. a cascade of reservoirs or a simplified physical system.

iii. Semi – distributed, physically – based models (SDMs): The catchment is divided into "functional" subparts, which can be areas that are homogeneous with respect to one or more characteristics (land use, soil type), or structural elements (slope, drainage network), or classes of points having the same hydrological behaviour (hydrological similarity concept). The fluxes are computed using physical equations with same assumptions and solved analytically.

iv. Distributed, process based numerical models (DPMs): The catchment is described using a grid (regular or not, square or not). The fluxes are computed using the partial differential equations of the physics of porous media and hydraulics, solved by a numerical scheme (finite differences or finite elements). The WBM model used in the present study falls under this category.

Four important hydrologic models are reviewed to understand the structure of the hydrologic models in terms of input and output data and the practical applicability of these models.

TOPOG

TOPOG is a research tool developed by a large group effort of *CSIRO (Commonwealth scientific and industrial research organisation) Land and water* and the *Cooperative*

Research Center for Catchment Hydrology, Australia, in 1986 for wide range of water and land management. It is a Hydrologic modelling package, which simulates the movement of water through the complex terrain. It explains the behaviour of hydrologic system based on physics behind it and hence, deterministic in nature. The model accounts for distributed parameters such as soil types, vegetation and climate by considering their spatial variability. It describes the movement of water over the surface, within the ground and evapoaration to the atmosphere. It also simulates the movement of solute through soil and sediment movement over the land surface. TOPOG is based on the WETZONE program, developed by Dr. Emmett O'Loughlin in the mid-1980. It has undergone several changes after that (http://www.per.clw.csiro.au/topog/intro/intro.html).

TOPOG enables the analysis of three-dimensional landscape through sophisticated digital terrain analysis. It is intended for small catchments (up to 10 km^2, and generally smaller than 1 km^2). It starts with raw contours and digital elevation model contours. The network is divided into cells by series of flow tubes, which diverges or converges, from the ridges and valleys on the catchment boundary. Depending upon the shape of the terrain, the contours change and hence, the density of the cells can be altered. The standard suggested cell size is 20 m by 20 m. The aspect, slope, equinox radiation, the summer radiation, etc. are needed to be entered for each cell. The TOPOG calculates the parameters related to steady state water balance such as normal wetness index, radiation-weighted index, and dynamic water balance parameters such as daily water balance, moisture storage, and water table depth and soil moisture.

STREAM

The Spatial tools for River basins and environment and analysis of management (STREAM) is a river basin management instrument. Originally, the RHINEFLOW (Kwadijk, 1993; van Deursen & Kwadijk, 1994) was developed to analyse the impact of climatic changes on the water resources availability of Rhine basin. STREAM is an extension over it and includes the effect of land use changes and coastal dynamics also. It is a spatial distributed hydrological model, which uses GIS data to calculate water balance in a large river basin.

STREAM uses land use maps, soil type map, monthly precipitations maps, monthly temperature maps and a digital elevation model as inputs. The area under study is divided into grids. The water balances for these grids are determined by deriving flow directions from DEM and by using Thornthwaite & Mather (1957) equation. During calculation, it is able to accounts for human interventions in terms of land use changes and external influences such as climatic changes. The model provides potential and actual evapotranspiration, soil water regime, aridity index, runoff regime and snow cover as an output. The model has been applied to many large basins, such as Ganges-Brahmaputra-Meghna, Rhine, Zambezi and Yangtze basins (Aerts, Kriek and Schepel, 1999).

The development of the model was done within the framework of the Indian – Netherlands water and coastal management cooperative programme. Aerts (2002) describes the objective of the work as to develop an instrument which can be used to give insight in the long term impacts of land use change, climate change, river basin management, population

pressure, economic development and on the future water demand and water availability in the Krishna basin of size 258,948 km^2. The resolution of the data set is of 1 square kilometer. The potential evapotranspiration was calculated using the Priestly – Taylor method using monthly global datasets for air temperatures, radiation, albedo, cloudiness, and elevation. The model produces water availability and aridity maps.

Surface Water Model

Utrecht University developed a surface water model for Orinoco river basin in South America, to provide Governments, Non government organisations (NGO's) and other stakeholders with comprehensible tools for rough impact assessment of planned human interventions in the river basin on surface water runoff (Schot et. al., 2001). The Orinoco River is the third largest river in the world having draining area of 830,000 km^2. Due to the unavailability of large data sets, the model developed by Van Deursen and Kwadijk (1994) was used; which requires little input data and can be applied to large river basins like Rhine and Ganges-Brahmputra.

In the model, the water balance consists of three storages, snow, soil water and groundwater. These storages are connected by six fluxes, precipitation, snowmelt, and evapotranspiration, groundwater recharge, rapid runoff and delayed runoff. There are five controls on these fluxes, which are temperature, maximum water storage capacity of the soil, crop coefficient, separation coefficient and recession coefficient. The model is based on mainly three assumptions. First is that water balance on a location only depends on

local conditions from the previous time step and there is no contribution from the other locations. Second assumption is that all runoff is assumed to leave the basin within one model time step. Third assumption says the precipitation falling at the end of a time step is considered as discharge for that time step.

Precipitation, temperature, maximum water storage capacity of the soil, crop coefficient, separation coefficient, and recession coefficient are used as input to calculate the water balance per cell of the raster GIS. The flow path of the runoff is decided using digital elevation model of the catchment. The runoff volume is calculated by multiplying the cell area with the runoff from each cell. By routing the accumulated runoff towards the outflow point, local drainage directions were determined. The output from the model is a time series of maps showing spatial distribution of flux or storage. The effect of human interventions on river discharge was studied by creating hypothetical dam and water diversion.

The WBM Model

The Water Balance Model (WBM) is a physically based, spatially distributed parameter, conceptual catchment hydrological model. It was developed by Prof. Manfred W. Ostrowski in 1992 at the Institute for Hydraulics and Water Resources Engineering, Darmstadt University of Technology, Germany. It has undergone several modifications after that by a group of researchers under his guidance. Since WBM has been employed in the present research work, the detailed description of the model is presented in Chapter 3.

Chapter 3

The WBM

3.1 General

This chapter presents the detailed description of WBM model and its component. The WBM uses raster element which represents a column having four layers. The four layers are:

1. Infiltration layer,
2. Root layer,
3. Transport layer,
4. Ground water layer.

In each raster element, a detailed simulation of the soil – vegetation – atmosphere – transfer - system (SVAT) has been applied which accounts for separation of precipitation into storage processes in a vertical column and runoff generation. Each element can be partly vegetated as well as partly urbanised. The vertical column with all layers is shown in Figure 3.1.

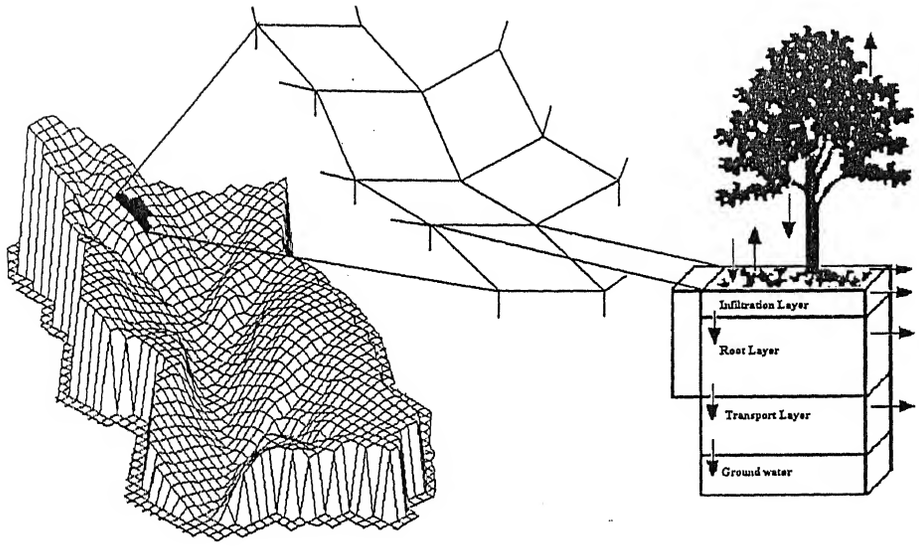

Figure 3.1: Vertical column considered for a raster element

A macro pore system is defined parallel to the first two layers i.e. infiltration layer and root layer. The Infiltration layer accounts for infiltration and evaporation. The root layer extends up to the maximum rooting depth of the plants and accounts for transpiration. In transport layer, water percolates to the ground water layer. The transport processes between adjacent elements through these layers are well explained in Figure 3.2. In case of high ground water level, capillary rise takes place in the root zone. Backwater effects have to be considered for lower two layers. Once the precipitation saturates the macro pore system and infiltration layer, surface runoff takes place. The lateral transport of the water is always unidirectional and follows the cascade system determined by surface topography.

For each elementary surface, the water balance is illustrataed with all relevant hydrological processes, so that, at each time and at each place, detailed evaluation can be possible.

3.2 Coupling with GIS

Topography based modelling started since 1990s. To model the transport process within the catchment, topographic information is necessary. Digital elevation model (DEM) provides such information automatically about the catchment area borders, catchment surfaces and direction of flow.

The Triangulated Irregular Network (TIN) model is a significant alternative to the regular raster of a DEM, and has been adopted in numerous GISs and automated mapping and contouring packages. In case of TINs or contour representations, sometimes, it is not possible to illustrate exactly the salient points like steep embankment of the catchment etc. Hence, raster format for the elementary surface is required which provides simple data storage and processing.

To administer the spatial distribution of the land use and parameters, which influences different processes, WBM model has been coupled with GIS. IDRISI is chosen as GIS program because of its comparatively simple data base management and user friendly routine. IDRISI was developed at Clark University. The model describing and model steering parameters are made available by providing different ASCII files to the program. The data structure and flow chart of the complete system of "IDRISI – WBM – FLIESS" is shown in Figure 3.2. The ability of IDRISI towards analysis of a digital elevation map (DEM) is limited, FLIESS was developed to performe a topopraphic analysis, and produce

ecaxtly the output that is needed for WBRM. FLIESS is a topographic analysis tool, that finds the flow paths through a DEM by the D8-Method with some additional modifications, delineates watersheds, gives the slope angles between raster grids and produces output for WBRM.

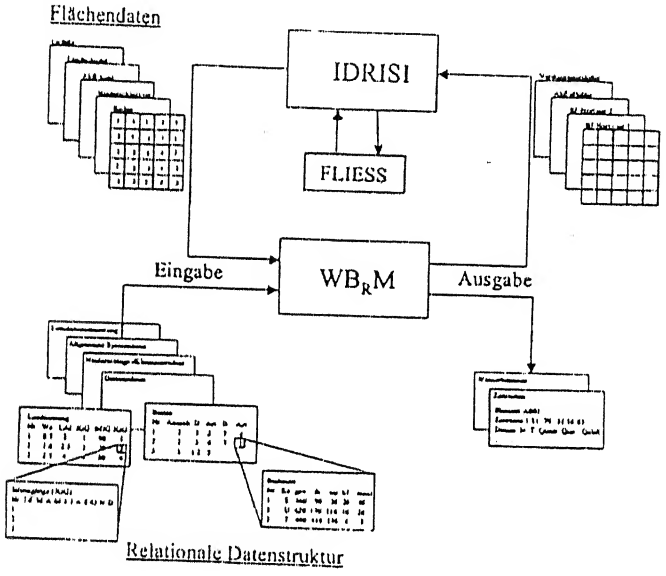

Figure 3.2: Flow chart of "IDRISI – WBM – FLIESS"

Note: Flachendaten means flat data, Eingabe means Input, Ausgabe means output, Relationale Datenstruktur means relational data structure.

3.3 Input and output of the WBM

To calculate the water balance, the following inputs are required at the desired time interval for which runoff is expected from the model. To mention the units of following

parameters, one hour is used as time interval. The WBM is flexible to incorporate any time interval. So the units will be changed accordingly.

i. Precipitation (mm)
ii. Temperature (^{0}C)
iii. Evapotranspiration (mm/hr)
iv. Digital elevation model
v. Classification of soil in the catchment
vi. Type of soil with their depth at a particular raster element
vii. Dimensions of the channel present in the catchment
viii. Land use characteristics.

The output from the model contains the values of following at an assigned time interval.

i. Through rainfall (mm)
ii. Interception evaporation and Interception (mm)
iii. Soil evaporation (mm)
iv. Transpiration (mm)
v. Evapotranspiration (mm)
vi. Soil moisture profile for different layers of soil
vii. Surface runoff (m^3/s)
viii. Base flow and groundwater recharge (m^3/s)
ix. Interflow (m^3/s)
x. Macropore flow (m^3/s)

3.4 Model components

Interception

When it rains over a catchment, not all the precipitation falls directly onto the ground. Before it reaches the ground, a part of it may be caught by the vegetation and subsequently evaporated. The volume of water so caught is called interception. Water may be retained by the vegetation as surface storage and returned to the atmosphere by evaporation. It can drip off the plant leaves to join the ground surface or the surface flow. The rainwater may run along the leaves and branches and down the stem to reach the ground surface. Change in Interception storage can be described using following function:

$$\frac{dS}{dt} = (1-p)N - D - E$$

Where, p: Passage coefficient; N: Precipitation; D: Drainage; E: Interception evaporation; S: Storage

Discharge component

Topographic information derived from DEM provides the basis for simulation of lateral water transportation. It has mainly three components – (1) the surface discharge, (2) the macropore storage and (3) the interflow. Each raster element receives water from its neighbours and passes on to its successors as shown in Figure 3.3. The arrows point to the successor.

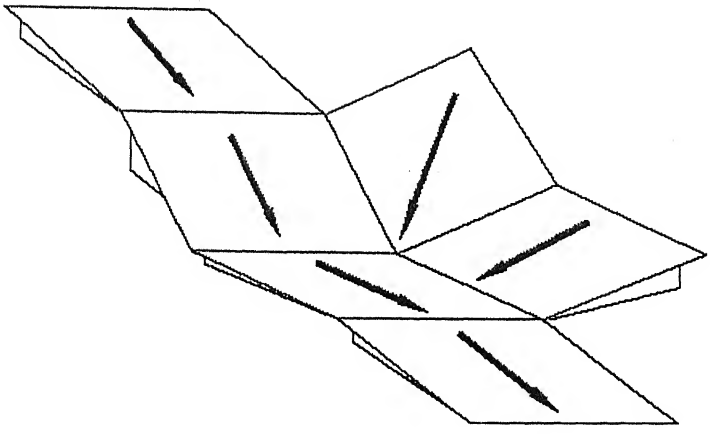

Figure 3.3: Cascade model of raster elements.

Surface discharge

Land surface discharge moves as layer discharge in small rivulets until a larger stream forms. Each raster element is covered with complete water film which flows off over the entire width of an edge as shown in Figure 3.4. The discharge behavior is described by continuity equation and Manning Strickler formula.

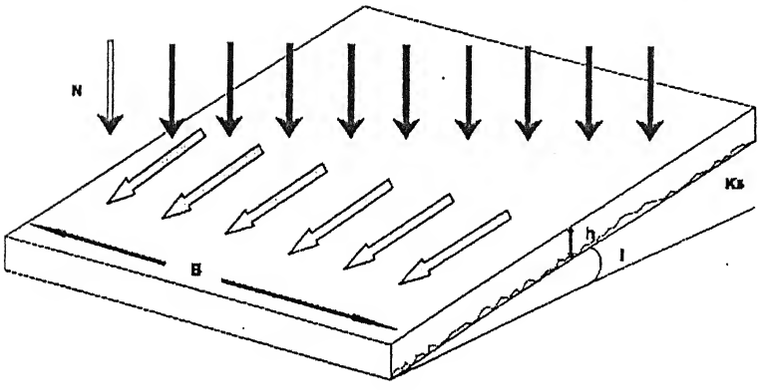

Figure 3.4: Schematic representation of a raster element

$$\frac{dh}{dt} = N_{eff} + \sum \frac{Q_z}{A} - \frac{Q_a}{A}$$

Where N_{eff} = Effective precipitation; Q_a = Surface discharge; Q_z = Lateral discharge; A = Surface area of the raster element; h = height of water film

$$V_m = K_s i^{1/2} h^{2/3}$$

Where V_m = Velocity of the flow; K_s = Roughness factor; i = download gradient as shown in Figure 3.4.

$$Q_a = V_m hB$$

Where B is the width of the discharge. Total discharge is counted on all elements of the catchment area whose surface exceeds a certain threshold value.

Macropore discharge

Capillary forces play a crucial role in macropore discharge. The description of the macropore system is very difficult to sieze. The size of the macropore system is expressed as percentage share of the total pore volume (TPV). Rain water, which cannot infiltrate into the soil matrix, first fills the macropore volume and when the capacity of the macropore is completely filled, it adds to the surface discharge.

Soil Moisture Simulation

A soil column consists of three homogeneous layers. Transportation of water from these layers is shown in Figure 3.5.

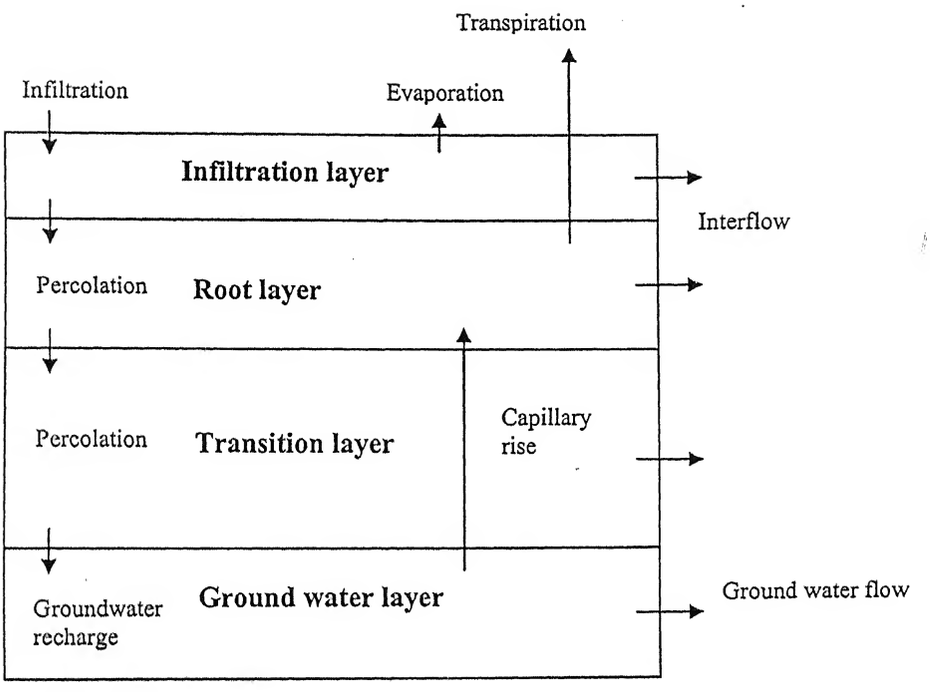

Figure 3.5: Transportation of rain water through Soil columns

The computation of water balance at time t is calculated from the following relation:

$$\frac{dM}{dt} = I(t) + K(t) - P(t) - If(t) - E(t) - T(t)$$

Where M = Soil Moisture (mm);

I(t) = rate of actual Infiltration (mm/h);

K(t) = rate of Capillary rise (mm/h);

P(t) = rate of actual exfiltration (mm/h);

If(t) = rate of actual Interflow (mm/h);

E(t) = rate of actual Evaporation (mm/h);

T(t) = rate of actual Transpiration (mm/h).

While calculating the soil moisture balance, it is to be noted that in layer 1, capillary term will be zero; in layer 2, Evaporation term will be zero; in layer 3, capillary, interflow, evaporation and transpiration term will be zero.

Infiltration

When water is applied to the surface of a soil, a part of it seeps into the soil. This movement of water through the soil surface is known as infiltration. The rate of infiltration has been calculated using following relationship:

$$I(t) = I_{\max} \cdot \left[\frac{f_2.FC - \theta(t)}{f_2.FC - f_1.FC} \right]^{1.4} + I_{end}$$

Where, θ = actual soil moisture [mm]; I_{max} = rate of maximum Infiltration [mm/h]; I_{end} = final rate of infiltration [mm/h]; f_1 = starting empirical factor; f_2 = final empirical factor; FC is field capacity.

For $\theta < f_1 * FC$, $I(t) = I_{max}$; For $\theta > f_2 * FC$, $I(t) = I_{end}$.

Percolation

To calculate the percolation, following equation has been used:

$$P(t) = Kf.\left[\frac{\theta(t) - f_1.FC}{f_2.FC - f_1.FC}\right]^{\alpha}$$

Where Kf = Saturated hydraulic conductivity [mm/h]; α = Soil type specific Exponent

Interflow

A part of the precipitation that infilters moves laterally through upper crusts of the soil and returns to the surface at some location away from the point of entry into the soil. This component of runoff is known as interflow.

To calculate the interflow, following equation has been used:

$$I(t) = \sin\beta.kf.\left[\frac{\theta(t) - f_1.FC}{f_2.FC - f_1.FC}\right]^{\alpha}$$

Where β = angle of inclination.

For $\theta < f_1 * FC$, $P(t)/I(t) = 0$;

For $\theta > f_2 * FC$, $P(t)/I(t) = \sin\beta * Kf$.

Capillary rise

The soil water is broadly classified into two categories: (1) Free water, and (2) Held water. Free water moves in the pores of the soil under the influence of gravity. The held water is retained in the pores of the soil, and it cannot move under the influence of gravitational force. Maximum rise of capillary has been calculated using following equation:

$$K(t) = 1 - \left[\frac{\theta(t) - f_1.FC}{f_2.FC - f_1.FC}\right].K_{max}$$

Where, K_{max} = Maximum rate of capillary rise [mm/h]

For $\theta < f_1 * FC$, $I(t) = K_{max}$;

For $\theta > f_2 * FC$, $I(t) = 0$.

Evapotranspiration

Evapotranspiration is the sum of evaporation and Transpiration. Evaporation comes from the highest layer (Infiltration layer). The maximum evaporation is reached with field capacity. Transpiration takes place from second layer and depends upon the available soil moisture. The following relations have been used to calculate these variables.

$$E(t) = E_{pot}.\left[\frac{\theta(t)}{FC}\right]$$

$$T(t) = [Ept - E(t)]\left[\frac{\theta(t) - WP}{FC - WP}\right]$$

With the knowledge of model components and required input data, the next chapters deals with the data processing to generate suitable data to apply the model to a catchment.

Chapter 4

Study area and data processing

4.1 General

In the present study, WBM model has been used to simulate various hydrological processes in Tarrawarra catchment, Australia. Due to sufficient online available data, the Tarrawarra catchment was selected which is located near Melbourne in Southern Victoria, Australia. In this chapter, first the description of the catchment along with available data has been presented; which will be followed by a brief description of the required inputs and obtained outputs from the WBM model.

4.2 Description of the catchment

The area of Tarrawarra catchment ($37^0 39'$ south, $145^0 26'$ east) is 10.5 hectares. The catchment has smoothly undulating terrain with no perennial streams and no channels. It has few 10 m cypress trees, 5 m mixed Australian native trees and two Eucalyptus trees. The vegetation cover is greater than 90%. The land is used for cattle grazing. A road follows along the northern boundary. The runoff from this road does not contribute to the catchment. The aerial photograph of the catchment looking south east is shown in Figure 4.1.

The climate is temperate with mean annual rainfall of 820 mm and potential evapotranspiration of 830 mm. The minimum and maximum mean temperatures in summer are 9^0C and 24^0C, respectively; and those for winter are 3^0C and 10^0C, respectively.

The soil in the catchment consists of 3 layers. At the upper slope of the catchment, it has typically 20 cm thick silty loam or silty clay loam A1 horizon, a silty clay loam A2 horizon and heavy clay B horizon. The midslope soils have a loam clay loam A horizon of 20 cm thick, which gradually transitions into a silty clay loam B horizon. The surface soil cracks during dry periods. The definition of different horizons can be found in Appendix B.

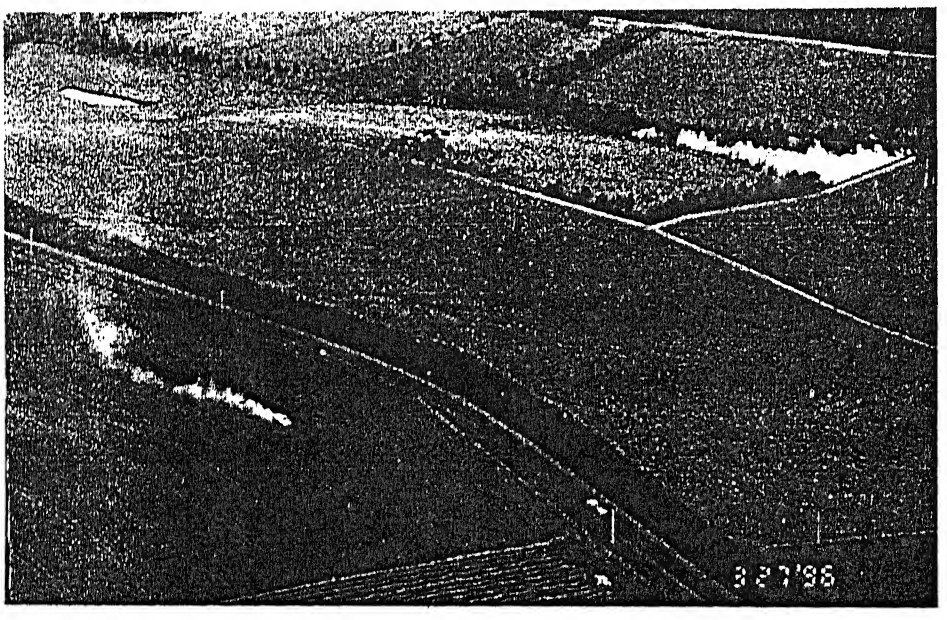

Figure 4.1: Aerial photo of Tarrawarra catchment looking south east

4.3 The Tarrawarra data set

The Tarrawarra data set are available on Dr. Andrew Western's home page, who is Senior Research Fellow in the Cooperative Research Center for Catchment Hydrology and Center for Environmental Applied Hydrology at the Department of Civil and Environmental Engineering at the University of Melbourne, Australia. It can be directly downloadable from the following link:

http://www.civag.unimelb.edu.au/~western/tarrawarra/tarrawarra.html.

The available data has been classified into 8 categories. The content of each file is shortly described below.

Topographic Data

A detailed topographic survey on a 10 m by 10 m paced grid was conducted within the local coordinate system using Total Stations. Two grided digital elevation models (DEM) of 5 m grid have been developed with Tarrawarra coordinate system and Universal Transverse Mercator (Zone 55).

Surface Soil Moisture Data

Soil Moisture maps of 10 m by 20 m grid have been collected using time domain reflectometry (TDR) over the top 30 cm soil layer. To ensure the accuracy of measured data, TDR data were calibrated with gravimetric measurement of soil moisture under some

typical field conditions. The data file contains date, time, point coordinates, dielectric constant and moisture data.

Soil Moisture Profile

Soil moisture profiles for 20 sites were measured using Campbell Pacific Nuclear 503 DR Neutron moisture meter over a period of 2 years. Measurements were taken by access tube at 15, 30, 45, 60, 90, 120 and 150 cm, depending upon the depth to bedrock. The site co-ordinates, depth to bedrock and soil profile description are available in 20 files.

Piezometer Data

Seventy four piezometers were installed to depths of between 0.5 m and 1.1 m to measure shallow water table elevations. Date, time and depth to water table from natural surface for 74 points are listed in a file.

Soil data

Saturated hydraulic conductivity, particle size data and soil profile data are available for the catchment. The soil profile data consists of point coordinates, the depth to the bottom of the A horizon (cm), the depth to the bottom of the B1 horizon (cm), the texture category of the B1 horizon, the depth to the bottom of the B2 horizon (cm), the texture category of the B2 horizon.

Metereological and Runoff Data

Meterological data from an automatic climate station and 5 collecting rain gauges are available at 6 min. interval for 3 consecutive years (1995 to 1997). The Meterological data consists of dry bulb air temperature, wet bulb air temperature, rainfall, average wind speed, maximum wind speed, wind direction, global radiation and net radiation. A separate file with daily summary of minimum, maximum and mean values of temperature, daily accumulation of rainfall and radiation variables, wind – run and maximum wind speed are available.

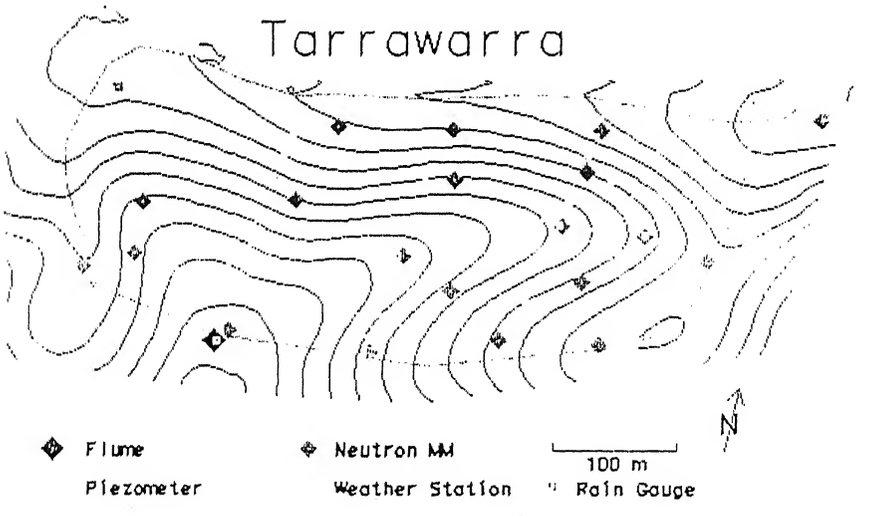

Figure 4.2: Tarrawarra catchment with contours lines and meteorological stations

To measure the surface runoff, a flume has been installed near the outlet of the catchment. The positions of climate stations, rain gauges and flume are shown in Figure 4.2. Water levels in the flume are measured every minute and are saved if the change in water level

exceeds 1.5 mm from the previous measurement. This means that if the change is less than 1.5 mm, then it is not recorded and it is assumed to be constant. With this logic, when the data are not available (means not recorded) then the actual value of flow is within 1.5 mm of the last recorded flow value. Therefore, the missing flow values can be assumed constant equal to the last recorded value.

Surface Roughness and Vegetation data

Vegetation was sampled from 1m by 1m plot. The vegetation consists predominantly of perennial and annual introduced grass and clover pasture species typical of Australian region. Sampling coordinates, water content and biomass in g/m^2 have been provided in a file. Surface roughness was measured using pin profiler having 41 pins at a spacing of 25 mm. Six profiles were measured at each site: two across the slope; two up the slope; and two at 45^0 to the slope.

Photographs and Maps of the catchment

Contour map, moisture maps, aerial photographs looking catchment from different directions, photographs of different instruments used in data acquisition was available.

4.4 Input files used in the model

The input files with their short description are presented below.

BNR_ATAR

The file contains information regarding region showing similar soil type in the catchment. The entire catchment has been divided into 20 different regions by assuming 20 different points and applying Theisen polygon method.

DHM_ATAR

This file contains DEM of the catchment as shown in Figure 4.3.

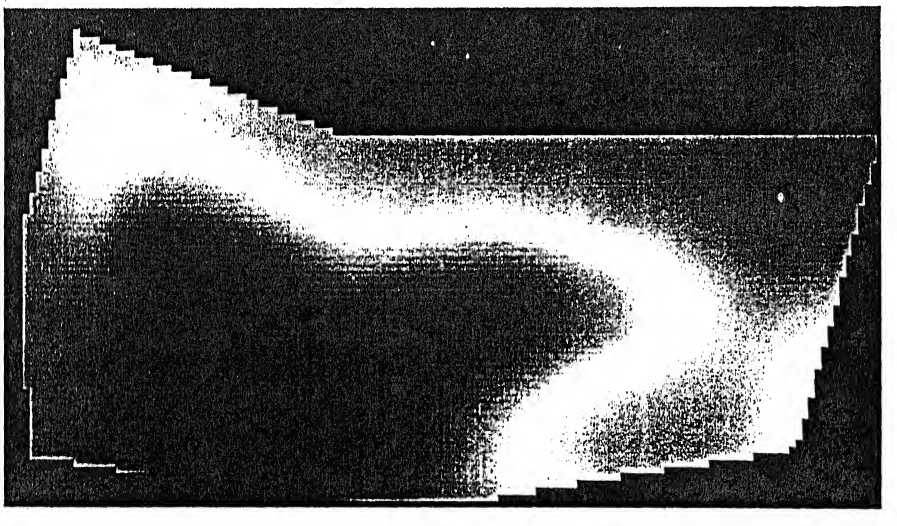

Figure 4.3: Digital elevation model of Tarrawarra catchment

GCA_ATAR

This contains information about the number of grid cells that are contributing flow to the actual grid cell.

GEF_ATAR

This provides information about the slope of a grid cell to its consecutive grid cell as an input to the model.

LNR_ATAR

This file contains information about the distribution of land uses.

NAC_ATAR

This conveys about the flow pattern to the model. This file contains information that how many grid cells are contained in each grid cell.

PZR_ATAR

This file contains information regarding the regions for which soil moisture profile is desired after simulation.

Weiras.AAW

The duration of simulation run with time interval is defined in this file.

Weiras.BOA

The type of soil within the catchment with their welting point, field capacity, saturated hydraulic conductivity and maximum infiltration is assigned in this file.

Weiras.BOD

The depth of soil layers with their type for all the categorised regions within the catchment is assigned here.

Weiras.EFE

In this file, user can define the information about number of different land uses with number of regions with similar soil types in the catchment. For example, in the present study, the entire catchment is considered having single type of land usage and the soil within the catchment has been divided into 20 regions.

Weiras.EFT

The threshold values necessary to form a channel is assigned here.

Weiras.EZG

This file associates the input time series of a catchment.

Weiras.FIL

The name of input rain, temperature and evapotranspiration file with their unit and time interval in which these data are available for the model.

Weiras.JGG

This file contains the factors by which the values of parameters assigned in Weiras.LNZ will be multiplied and results into the new values of parameters for different month.

Weiras.LNZ

The root depth, vegetation cover and its seasonal variations, leaf area index and its seasonal variation, percentage of unproductive land, surface roughness value and Haude monthly coefficient for evapotranspiration is assigned in this file.

Weiras.TRS

The geometry of channel is specified here in this file.

4.5 Generation of input files from available data

The required input files along with its preparation from available data has been discussed in this section.

4.5.1 Soil classification

The soil profile data of catchment was available. The available data files looks like as follows.

X coord m	y coord m	A horizon depth to bottom cm	B1 horizon depth to bottom	B1 horizon texture category	B2 horizon depth to bottom cm	B2 horizon texture category
805	950	24	39	clay	>72	clay
805	930	24	46	clay	>75	clay
805	910	16	51	clay	>74	clay

B1 horizon texture was taken as reference to categorise the available data into three types of soil – clay, silt and silt clay. The depth of layers was calculated from here. Twenty points were chosen out of this data set and used to create BNR_ATAR file. The generated output BNR file is shown in Figure 4.4.

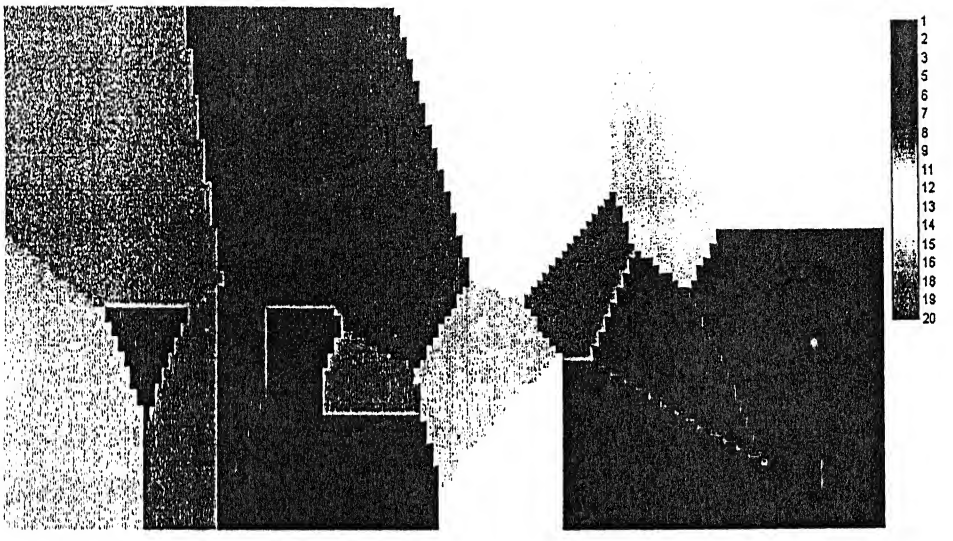

Figure 4.4: Regions with different soil types

The soil classification with information about different layers has been provided in Weiras.BOD file. The input Weiras.BOD for the present study is shown below.

Boden (*.BOD)

ID	Boden-Kenngroessen														GW Stand	Beschreibung
	mak	anzsch	d1	boa1	d2	boa2	d3	boa3	d4	boa4	d5	boa5	d6	boa6		
-	mm	-	m	-	m	-	m	-	m	-	m	-	m	-	m	-
1		3	0.21	2	0.18	3	0.36	3								Boden I
2		3	0.19	2	0.24	3	0.32	3								Boden II
3		3	0.26	2	0.27	2	0.22	3								Boden III
4		3	0.25	2	0.22	2	0.28	3								Boden IV
5		3	0.19	2	0.24	2	0.32	3								Boden V
6		3	0.19	2	0.36	2	0.20	1								Boden VI
7		3	0.19	2	0.29	2	0.27	1								Boden VII
8		3	0.25	2	0.30	2	0.20	1								Boden VIII
9		3	0.22	2	0.27	2	0.27	1								Boden IX
10		3	0.24	2	0.14	2	0.37	2								Boden X
11		3	0.21	2	0.22	1	0.32	3								Boden XI
12		3	0.22	2	0.22	1	0.31	3								Boden XII
13		3	0.17	2	0.15	1	0.43	3								Boden XIII
14		2	0.25	2	0.50	3										Boden XIV
15		2	0.22	2	0.53	3										Boden XV
16		2	0.26	2	0.49	2										Boden XVI
17		2	0.24	2	0.51	2										Boden XVII
18		2	0.30	2	0.45	2										Boden XVIII
19		2	0.29	2	0.46	2										Boden XIX
20		2	0.23	2	0.52	1										Boden XX

Note: Boden means soil; Beschreibung means description; boa1, boa2 indicates the types of soil and d1, d2 are depths of different soil layers.

4.5.2 Rainfall

There were five rain gauges installed in the catchment to measure rainfall. The rainfall data along with other meteorological data at 6 min interval was available for three years 1995, 1996 and 1997. The daily summary of the meteorological data was also available in a separate file. To verify the uniformity of rainfall throughout the catchment, it was necessary to compare the available rainfall data for all five rain gauges. The time series graph showing rainfall from different rain gauges are shown in Figure 4.5. This figure clearly indicates that the rainfall can be assumed to be uniform for whole catchment. Rainfall values in the required format were prepared to provide as an input to the model.

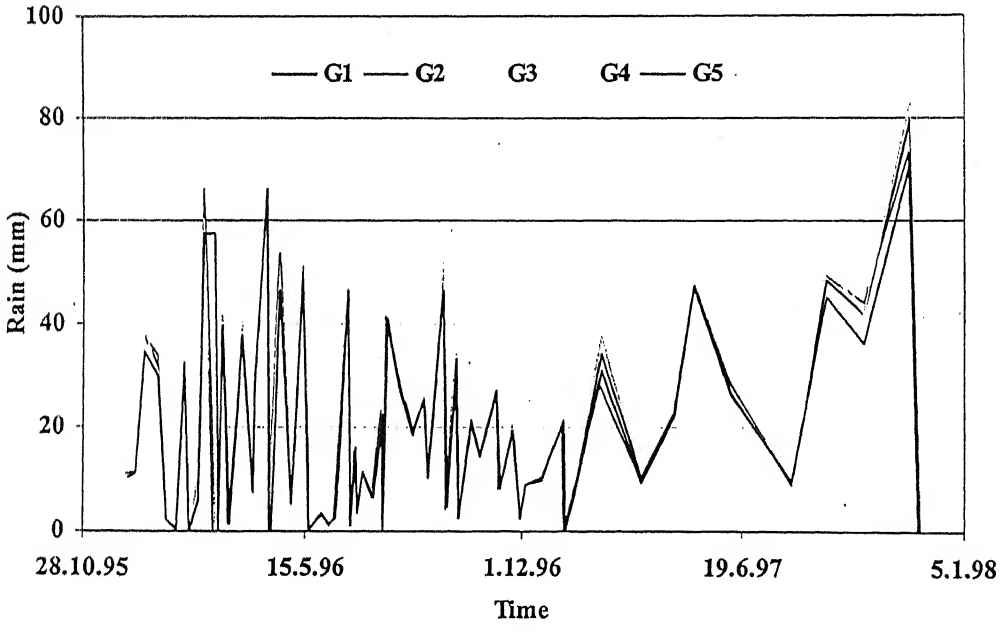

Figure 4.5: Time series graph of available rainfall

4.5.3 Temperature

The dry bulb air temperature, wet bulb air temperature, surface air temperature were available. The surface air temperature has been used in the model.

4.5.4 Evapotranspiration

The meteorological data were used to calculate evapotranspiration using Pennmann Monteith Equation which has been described later in this chapter.

4.5.5 Runoff

Instantaneous surface runoff values for three years were available. The available data set of observed surface runoff looks as follows.

```
Units: runoff is in mm/h
20/10/95 8:30:00  0.0194
20/10/95 8:49:00  0.0172
20/10/95 9:03:00  0.0148
20/10/95 9:09:00  0.0127
20/10/95 9:35:00  0.0105
20/10/95 10:00:00 0.0081
20/10/95 10:43:00 0.0069
20/10/95 11:28:00 0.0059
```

In the present case the defined time interval was 6 min. So, the obtained surface runoff from model was at 6 min interval only. To compare the time series graph, it was necessary to extract data of observed surface runoff at 6 min. interval. From the available data set, the values which were lying at time step which are multiple of 6 min. were only captured and

others were discarded. e.g. out of data set shown above, the captured surface runoff values will be at 8:30 and 10:00, because only these times are falling at a multiple of 6 minute. The observed surface runoff directly drawn from available data and the extracted observed surface runoff are shown in Figure 4.6a and Figure 4.6b, respectively. By observing these two figures, it is clear that the information has not been lost due to this methodology to extract the available data as per the required format.

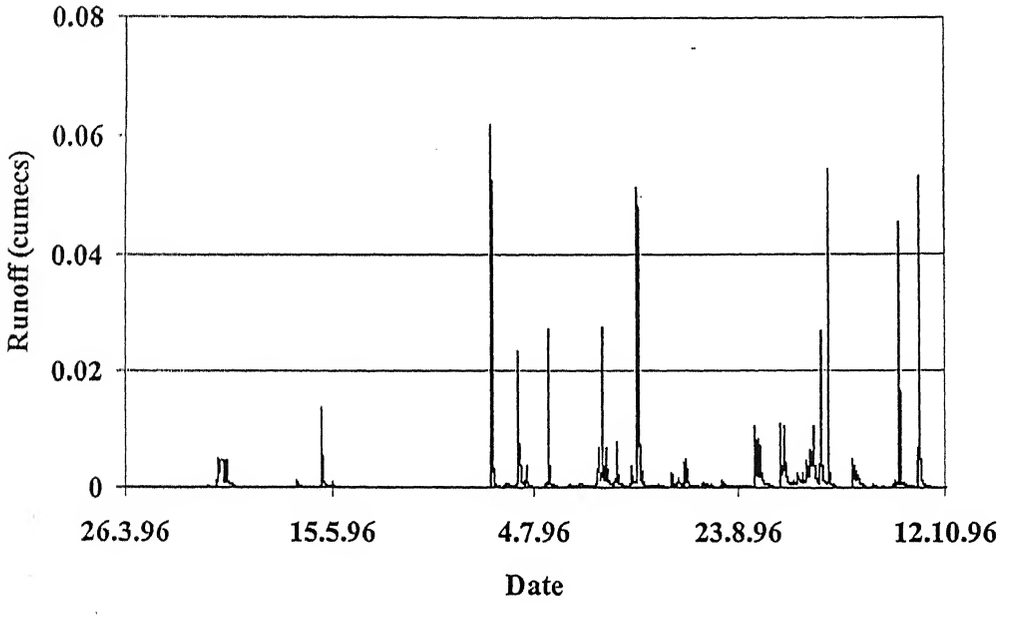

Figure 4.6a: Time series from the available observed data

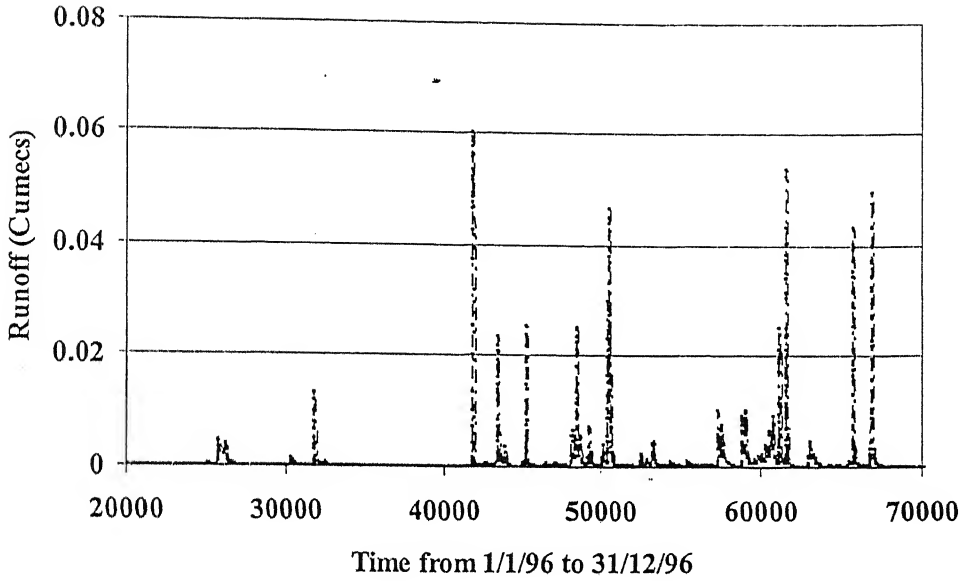

Figure 4.6b: Time series from extracted data

4.6 Output files obtained from the model

There are six folders in which output values are stored after the model run.

i. OUTWEL

ii. BODFUN

iii. OUTSMU

iv. OUTWBM

v. OUTPZR

vi. OUTRST

In OUTWEL folder, all the meteorological information is stored. Most of the times, the output files stored in this folder is only required for analysis of simulation results. For further and deep investigation of results in terms of movement of water in soil layers and to the atmosphere, one needs to check files stored in the other folders.

BODFUN contains file which shows functions generated for infiltration, exfiltration rates and percolation with available soil moisture (refer to Figure 5.11). The data files stored in OUTPZR folder presents values for soil moisture in volume % for all the defined points in pzr_atar file and at assigned time interval. OUTRST contains soil moisture profile in raster format as per the information provided in the weiras.EFT file.

4.7 Data Processing

The Meteorological data are reported to be available for three years; but actually these are available for the following period with lot of missing values.

Year 1995: 10/8/95 to 31/12/95

Year 1996: 1/1/96 to 31/12/96

Year 1997: 1/1/97 to 17/11/97

By deep investigation of the available data, the following five periods were determined, in which the continuous 6 minutely meteorological data are available. The periods are mentioned below:

Period 1: 12:06 on 26/6/96 to 23:54 on 3/7/96;

Period 2: 00:00 on 17/7/96 to 21:24 on 11/8/96;

Period 3: 00:00 on 24/8/96 to 12:06 on 31/8/96;

Period 4: 09:30 on 2/9/96 to 04:06 on 16/9/96;

Period 5: 00:00 on 30/9/96 to 12:48 on 8/10/96.

The runoff values in this period were almost continuous except some periods. The missing runoff data were filled using linear interpolation. To run the model, evapotranspiration values at 6 minute interval for these periods were required. The widely used Penman – Monteith equation calculates the evapotranspiration values only at the daily basis. To apply the Penman – Monteith equation on an hourly or shorter time scale, the equation needs to be adjusted. Smith (1992) suggests the Penman-Monteith equation for hourly time step as:

$$ET_0 = \frac{0.408\Delta(R_n - G) + \gamma . \frac{37.5}{T_{hr} + 273} u_2 (e^0(T_{hr}) - e_a)}{\Delta + \gamma(1 + 0.34u_2)}$$

ET_o is the reference evapotranspiration (mm hour^{-1});

R_n is the net radiation at the grass surface (MJ m^{-2} hour^{-1});

G is the soil heat flux density (MJ m^{-2} hour^{-1});

T_{hr} is the mean hourly air temperature (°C);

Δ is the saturation slope vapour pressure curve at T_{hr} (kPa °C^{-1});

γ is the psychrometric constant (kPa °C^{-1});

$e°(T_{hr})$ is the saturation vapour pressure at air temperature T_{hr} (kPa);

e_a is the average hourly actual vapour pressure (kPa);

u_2 is the average hourly wind speed (m s^{-1}).

Evapotranspiration values at 6 minute interval can be calculated using above equation by changing factor from 37.5 to 3.75 in the second term of numerator. The other variables also need to be provided at 6 minute interval in order to get result at 6 minute interval.

So, the equation becomes,

$$ET_0 = \frac{0.408\Delta(R_n - G) + \gamma.\frac{3.75}{T_{hr}+273}u_2(e^0(T_{hr}) - e_a)}{\Delta + \gamma(1 + 0.34u_2)}$$

Given relative humidity measurements, the actual vapour pressure is determined as:

$$e_a = e^0(T_{hr})\frac{RH_{hr}}{100}$$

Where, e_a is the average actual vapour pressure (kPa); $e°(T_{hr})$ is the saturation vapour pressure at air temperature T_{hr} (kPa); RH_{hr} is the average hourly relative humidity (%).

$$e^0(T) = 0.6108.\exp\left[\frac{17.27 * T}{T + 237.3}\right]$$

Where, e°(T) is the saturation vapour pressure at air temperature T (kPa) and T is the air temperature (°C).

$$\Delta = \frac{4098 * \left[0.6108 \exp \frac{(17.27 * T)}{T + 237.3}\right]}{(T + 237.3)^2}$$

Where Δ is saturation slope vapour pressure curve at T (kPa $°C^{-1}$);

$G = 0.1 * R_n$ during daylight periods; $G = 0.5 * Rn$ during night time periods.

4.8 Calibration and Validation data set

The minimum, maximum and standard deviation of relative humidity, ground temperature, rainfall, wind speed, runoff and net radiation for above mentioned 5 different periods are tabulated below.

	RH	GRND	RAIN	WIND	Runoff	Net.Rad.
	%	TEMP	6min	6min	M3/sec	
	*	Mean	total	mean		mean
	calc	^0C	mm	kph		W/m^2
Period 1: 12:06 on 26/6/96 to 23:54 on 3/7/96 (Total data: 1799)						
Max	97	15.3	1.2	23.8	0.0235	337.8
Min	87	2.3	0	0.4	0.00	-80.2
Average	91.93	9.29	0.01	6.12	0.0013	11.90
Std deviation	1.69	2.45	0.07	4.65	0.0026	71.46
Period 2: 00:00 on 17/6/96 to 21:24 on 11/8/96(Total data: 6211)						
Max	94	16.5	1	38.3	0.0511	427.8
Min	38.00	1.50	0.00	0.40	0.0000	-81.50
Average	80.37	9.18	0.01	7.85	0.0018	14.96
Std dev	8.08	2.66	0.06	5.51	0.0045	79.67
Period 3: 00:00 on 24/8/96 to 12:06 on 31/8/96(Total data: 1802)						
Max	93	19.1	0.6	20.8	0.0104	471.7
Min	52	2.9	0	0.4	0.0000	-79.3
Average	77.67	10.53	0.01	5.00	0.0012	37.86
St dev	10.62	3.34	0.06	3.60	0.0019	109.35

Period 4: 09:30 on 2/9/96 to 4:06 on 16/9/96(Total data: 3306)						
Max	91	19.1	2.2	41.6	0.0541	578.6
Min	48.00	3.40	0.00	0.40	0.0000	-75.70
Average	74.66	9.98	0.02	10.31	0.0027	43.55
St dev	9.11	2.76	0.09	6.49	0.0048	115.34
Period 5: 00:00 on 30/9/96 to 12:48 on 8/10/96(Total data: 2047)						
Max	92	23	1.4	31.1	0.0531	747.6
Min	42.00	5.60	0.00	0.40	0.0000	-71.40
Average	73.25	12.22	0.02	8.41	0.0017	78.07
St dev	11.36	3.39	0.08	5.53	0.0046	162.32
Overall (Total data: 15165)						
Max	97	23	2.2	41.6	0.0543	747.6
Min	38	1.5	0	0.4	0.0000	-81.5
Average	79.22	9.94	0.01	7.93	0.0061	32.07
Std Dev	10.26	3.03	0.07	5.71	0.0102	107.55

By investigating the above statistics, two periods were selected for further analysis, (1) Period-4 (total data points 3306) for calibration and (2) Period-2 (total data points 6211) for validation.

It seems that Period 1 and period 3 are of limited range only, so these periods were not considered for further study. The time series plot for calibration and validation periods are shown in Figure 4.7a and Figure 4.7b respectively.

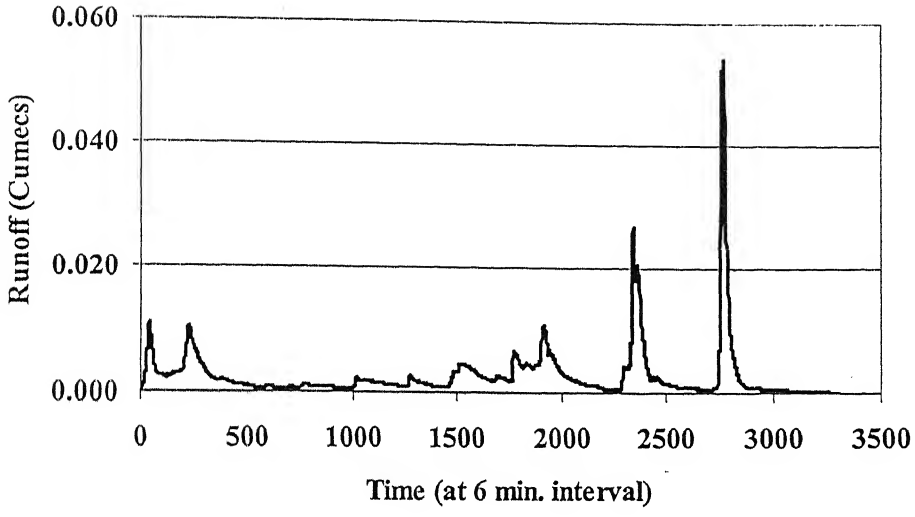

Figure 4.7a: Time series plot for calibration period

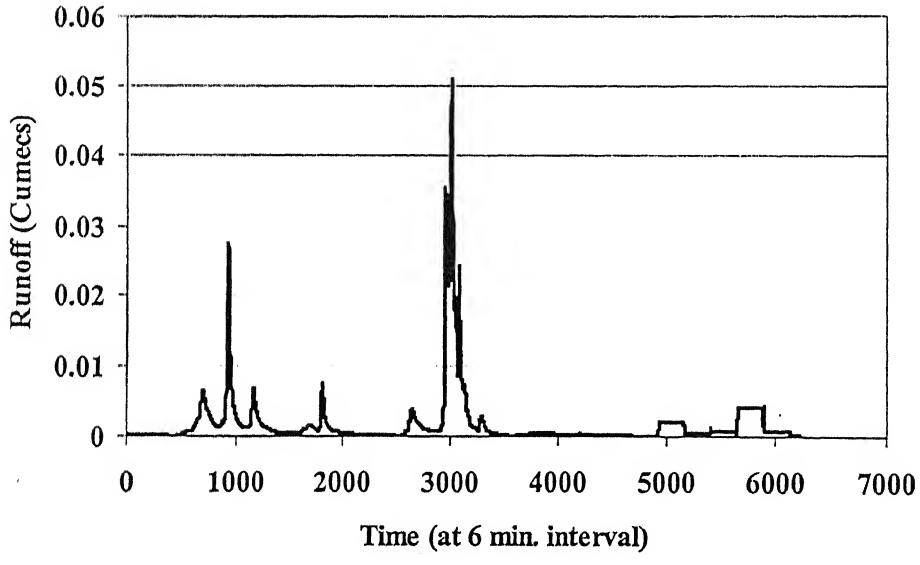

Figure 4.7b: Time series plot for validation period

The calibration period-4 was further classified into 3 sets on the basis of low peak flow (denoted by period 4L), medium peak flow (denoted by period 4M) and high peak flow (denoted by period 4H). The periods are as follows:

Period 4L: 9:30 on 2/9/96 (1) to 11:24 on 4/9/96 (500);

Period 4M: 18:24 on 11/9/96 (2250) to 10:24 on 13/9/96 (2650);

Period 4H: 15:24 on 13/9/96 (2700) to 21:30 on 14/9/96 (3001).

The numbers in the bracket corresponds to the number used to show time at 6 min Interval on the x-axis of the graphs shown in Figure 4.7a and Figure 4.7b.

Similarly the validation period were also divided into 3 categories. The periods are as follows:

Period 2L: 10:12 on 24/7/96 (1783) to 13:24 on 27/7/96 (2535)

Period 2M: 16:54 on 20/7/96 (890) to 17:42 on 21/7/96 (1138)

Period 2H: 4:24 on 29/7/96 (2925) to 20:24 on 30/7/96 (3325)

Chapter 5

Parameter estimation

5.1 General

Increasingly sophisticated computer-based hydrologic models are currently used in a variety of tasks. These hydrologic models must be calibrated to be useful for the solution of practical problems. Through calibration, we estimate values for the model parameters, which enable the model to closely match the behaviour of represented real system (watershed). It is generally believed that appropriate values, for certain model parameters, can be determined through direct measurements conducted on the real system. However, in many situations, the model parameters are conceptual representations of abstract physical characteristics and must be adjusted through a trial and error process that matches the model response to historical input output data.

There is no universal systematic procedure for model calibration. In this section, a particular sequence of calibration procedure is discussed, which has been adopted in the present work. The idea behind calibration of the model is to estimate the following seven parameters:

i. Infiltration rate (K_f) of silt clay in (mm/hr)

ii. K_f of silt in (mm/hr)

iii. K_f of clay in (mm/hr)

iv. Maximum infiltration rate of silt clay in (mm/hr)

v. Maximum infiltration rate of silt in (mm/hr)

vi. Maximum infiltration rate of clay in (mm/hr)

vii. Roughness (K_{st})

The values of these parameters should be chosen in such a fashion that the output runoff from the model should approximately match with the observed runoff. The optimum values of these parameters were desired. Root mean square error (RMSE), normalised root mean square error (NRMSE), Nash Sutcliffe Efficiency (E), Coefficient of efficiency (E1), Correlation coefficient (R), average absolute relative error (AARE) and sum squared error (SSE) were also calculated while calibration and validation of the model. These error statistics can be calculated using following equations.

$$RMSE = \sqrt{\frac{1}{N}\sum (Q_{obs} - Q_{cal})^2} \tag{1}$$

$$NRMSE = \frac{\sqrt{\frac{1}{N}\sum (Q_{obs} - Q_{cal})^2}}{\frac{1}{N}\sum Q_{obs}} \tag{2}$$

$$E = 1 - \frac{\sum (Q_{cal} - Q_{obs})^2}{\sum (Q_{obs} - \overline{Q_{obs}})^2} \tag{3}$$

$$E1 = 1 - \frac{\sum |Q_{obs} - Q_{cal}|}{\sum |Q_{obs} - \overline{Q_{obs}}|} \quad (4)$$

$$R = \frac{\left[\sum \left((Q_{obs} - \overline{Q_{obs}}) * (Q_{cal} - \overline{Q_{cal}})\right)\right]^2}{\sum (Q_{obs} - \overline{Q_{obs}})^2 * \sum (Q_{cal} - \overline{Q_{cal}})^2} \quad (5)$$

$$AARE = \frac{1}{N} \sum \left| \frac{Q_{cal} - Q_{obs}}{Q_{obs}} \right| * 100 \quad (6)$$

$$SSE = \sum (Q_{cal} - Q_{obs})^2 \quad (7)$$

$$MBE = 100 * \frac{\sum (Q_{cal} - Q_{obs})}{\sum Q_{obs}} \quad (8)$$

The step-wise procedure adopted in calibration of the model is described below.

First of all, select data set for which maximum numbers of continuous runoff, rainfall, temperature and meteorological data to calculate evapotranspiration are available at 6 minute interval. Then divide the data set for smaller periods so that model run should not take much time. To begin with, assign a guess value for the above mentioned 7 parameters and run the model. Draw time series graph with observed and calculated data and calculate error statistics. Check the sensitivity of all the parameters and accordingly decide the value of the parameters. Apply the selected combination of parameters for another period and check the time series and error statistics. Once the best match in time series is

obtained the combination of parameters will be declared as optimal from trial and error procedure.

5.2 Calibration using 1995 data set

First the model calibration was tried with the available data for 1995. There were two different data sets in which the data were continuous. The results obtained while calibrating the model using these data set are presented below.

5.2.1 Trial 1

The period chosen for this case study was from 8:30 on 20/10/95 to 7:00 on 22/10/95. Arbitrary combinations of seven parameters were tried. For each combination, time series graph for observed and predicted runoff were drawn in one sheet. Fifteen different combinations of values were tried. The best match in time series graph was observed for the values mentioned in Table 5.1. The time series plot for this combination is shown in Figure 5.1.

Table 5.1: Best combinations achieved from arbitrary selection

K_f (mm/hr)	Maximum Infiltration (mm/hr)	K_{st}
4.5	4.6	
4.5	4.6	3.0
0.05	0.06	

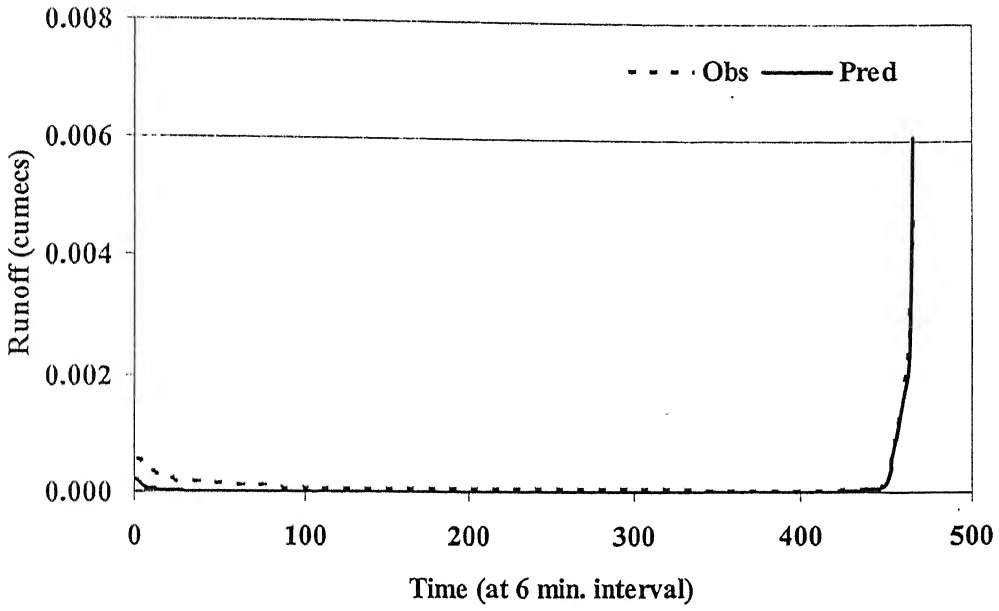

Figure 5.1: Time series graph for trial 1

The predicted runoff patterns were similar to the observed runoff. For better observation, it was necessary to increase the duration from 2 days to longer periods. Next the sensitivity of K_{st} was decided to observe.

The values of K_{st} were varied from 1 to 9.0 (1.0, 2.0, 2.5, 2.7, 2.8, 3.0, 3.5, 7.0, 9.0) to achieve match in peak runoff value. Few typical effects are presented in Figure 5.2a to Figure 5.2d. For smaller values of K_{st}, the predicted runoff was not following the patterns. For higher values (5.0, 7.0, 9.0), the predicted peak runoff were very high compared to observed runoff peak value and after certain point it started decreasing. The similarity in time series was observed for K_{st} values ranges from 2.0 to 3.5. Root mean square error

(RMSE) for each trial were calculated and it was found to be minimum for the K_{st} value of 3.0.

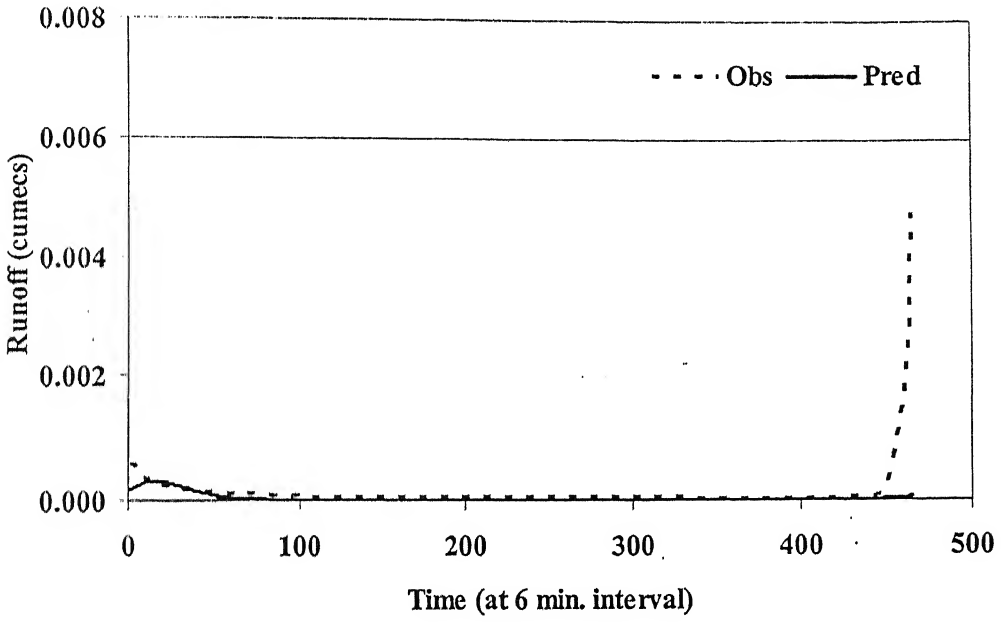

Figure 5.2a: Time series graph for K_{st} of 1.0

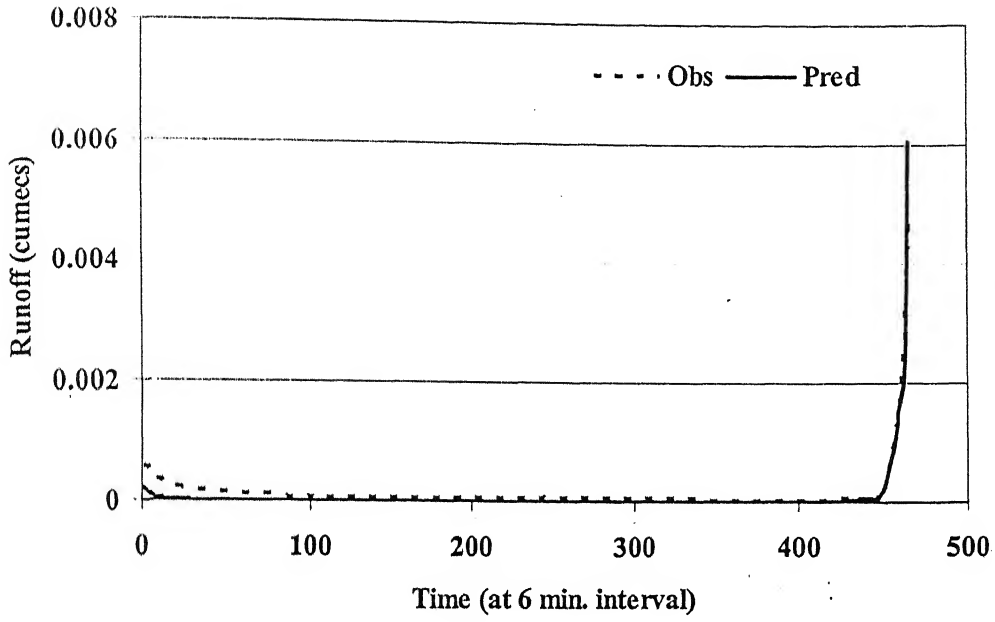

Figure 5.2b: Time series graph for K_{st} of 3.0

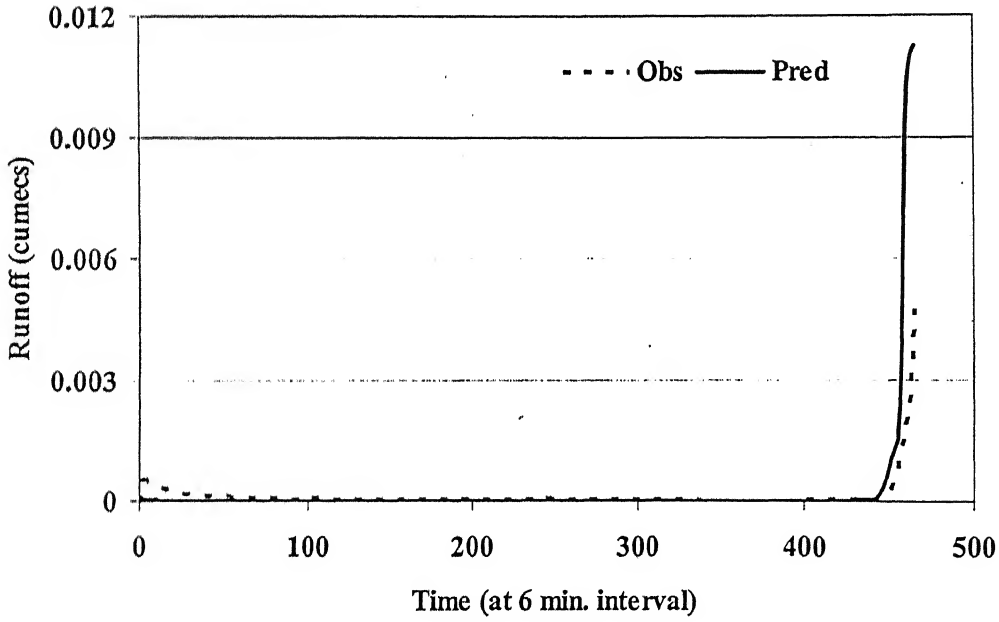

Figure 5.2c: Time series graph for K_{st} 5.0

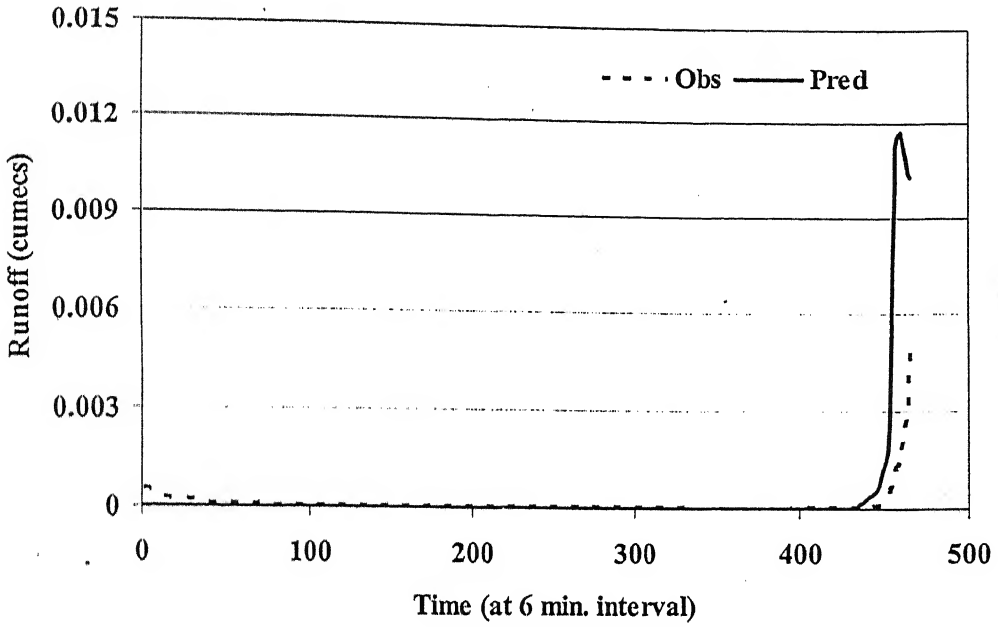

Figure 5.2d: Time series graph for K_{st} 9.0

With the K_{st} value fixed as 3, the peak was almost matching but at initial period, the pattern was shifted downward (clear from Figure 5.2b). So, to get the best fit in time series plot, the variation in values of other variables was tried by keeping K_{st} fixed as 3.0. By observing the RMSE values for each combination, it was clear that the combination selected earlier was the best.

From this analysis, the following conclusions could be drawn:

1) Best values of parameters are as given in Table 5.1
2) The study period should be increased or changed to observe the complete effect and to ensure the validity of chosen combination.

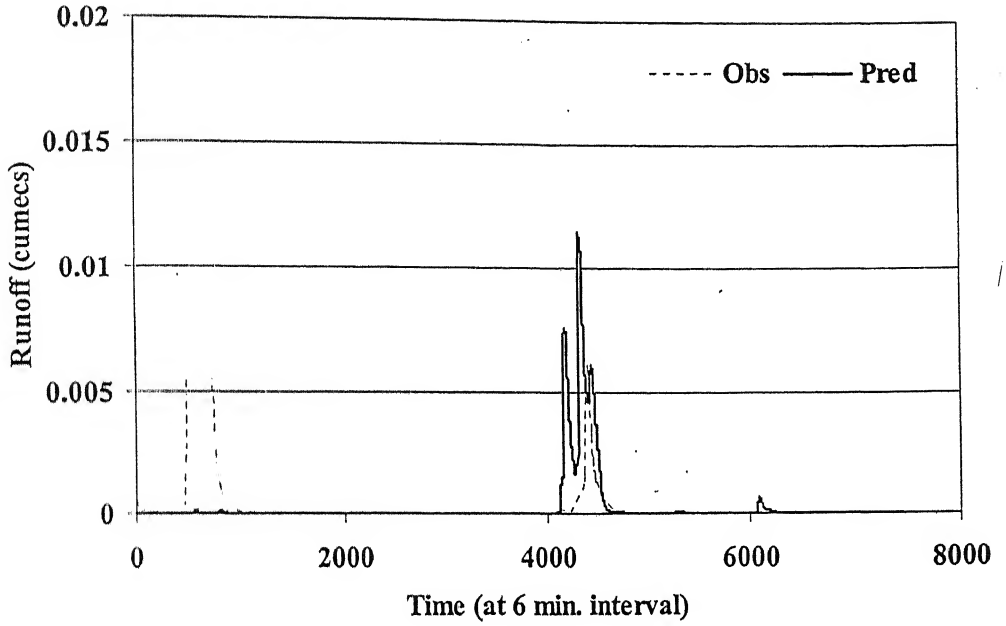

Figure 5.3a: Time series plot for K_{st} 0.5 and trial 2.

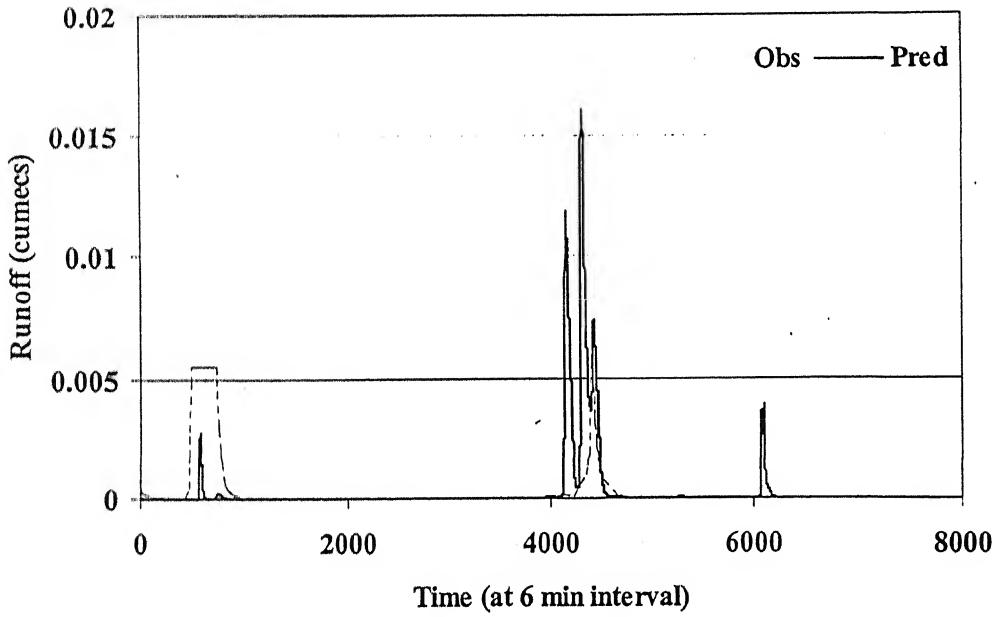

Figure 5.3b: Time series plot for K_{st} 0.8 and trial 2.

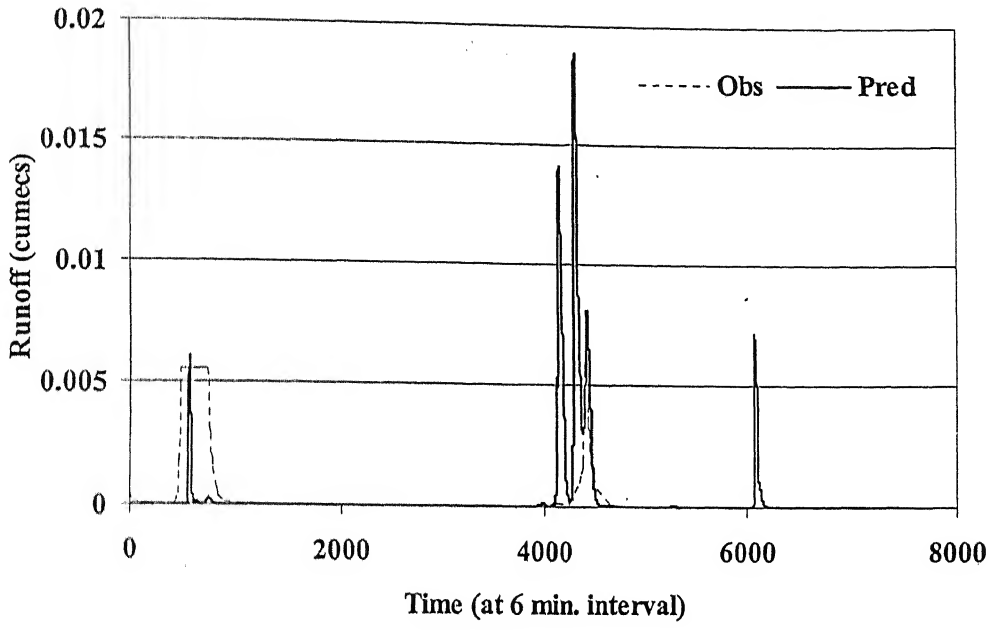

Figure 5.3c: Time series plot for K_{st} 1.0 and trial 2

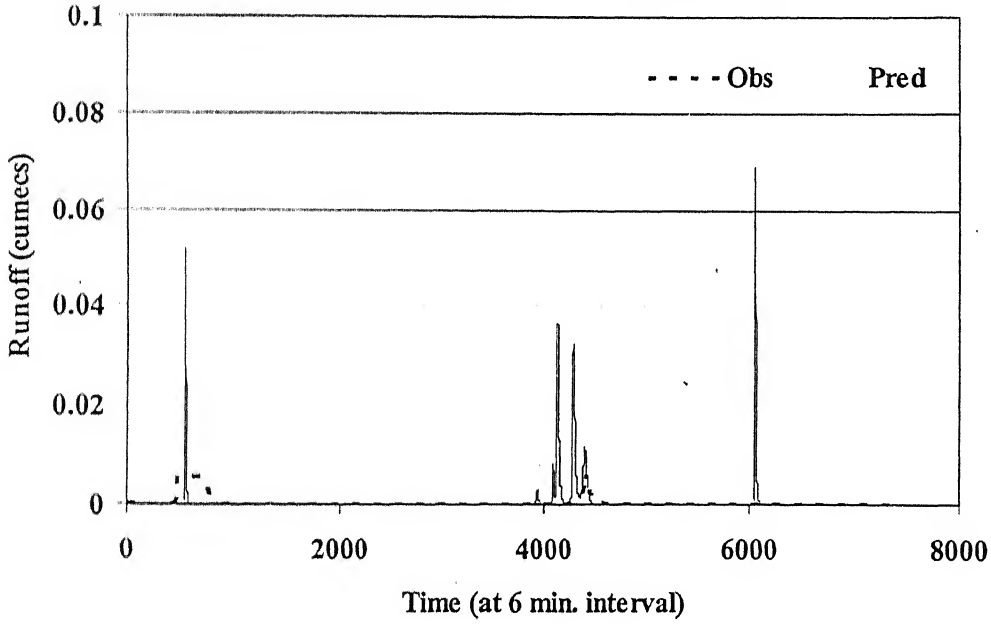

Figure 5.3d: Time series plot for K_{st} 3.0 and trial 2

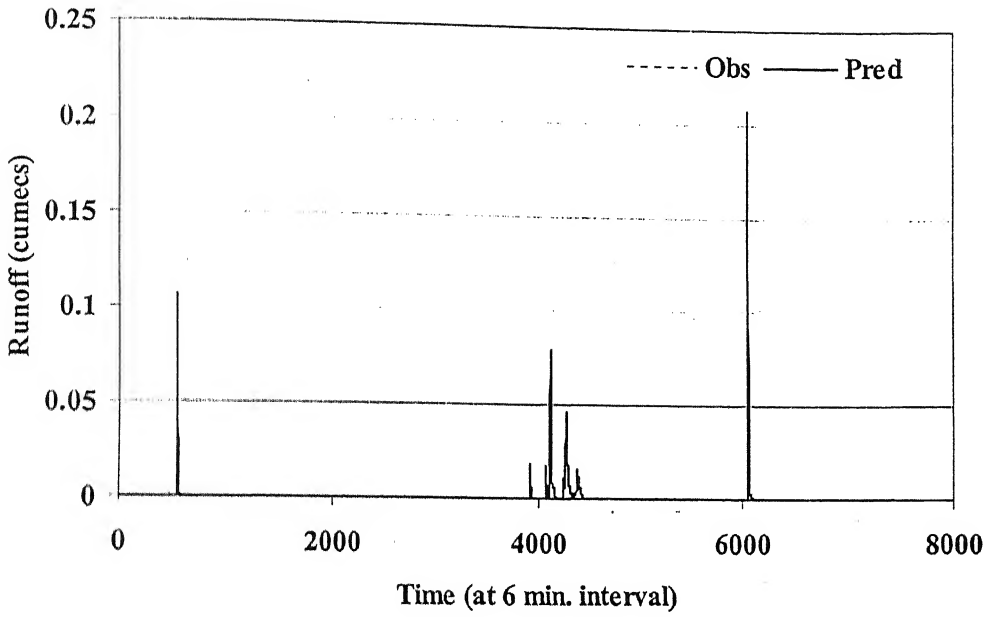

Figure 5.3e: Time series plot for K_{st} 9.0 and trial 2

It was decided to use the data set for which data of observed runoff for longer duration is available. From the available data set, the observed runoff data for 1996 was found to be suitable. So, the next calibrations were done using runoff values measured for year 1996.

5.3 Calibration using 1996 data set

The available data for 1996 were used to calibrate the model. There were three different periods in which most of the data were continuous. The results obtained while calibrating the model using these data set are presented below.

5.3.1 Data of 1996 Set 1

For this trial, the study period was from 00:00 on 1/5/96 to 12:18 on 18/6/96. In this period, only two peaks were there in the plot of time series graphs from observed data set. The objective to be attained during calibration was same as mentioned earlier. The earlier chosen values of parameters were used to note the effect. The time series graph is shown in Figure 5.4.

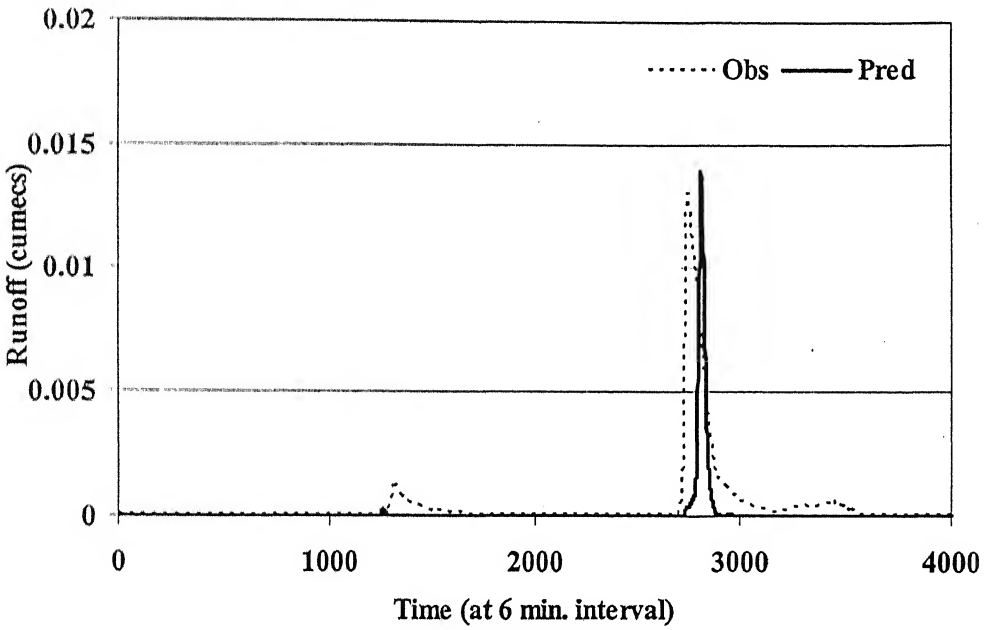

Figure 5.4: Time series plot for 96set1

Some remarkable points from this plot are time to start of rising limb was matching; time at the end of falling limb is not matching; the measured peak runoff values are slightly higher than observed value; the base time period of hydrograph obtained from model is less than that for the observed hydrograph.

It is clear from Figure 5.4 that the volume of runoff obtained from the observed hydrograph is higher than that obtained from the model. So decrease in the infiltration rate could be one of the solutions. But this will certainly result into an increase in peak value. So, another possibility could be to make the ground surface rough, so that it will allow the surface runoff to stay long and provide sufficient time to percolate. Different combinations of values were tried by decreasing the infiltration rates as well as by increasing the roughness values; but the desired similarity in hydrographs could not be achieved.

Up until now, the infiltration values for clay were kept very small. So, it was necessary to check its sensitivity. By increasing the infiltration rate for clay and decreasing the same for silt clay and silt form the earlier selected data, it was observed that the peak disappeared. So, it could be deduced from here that by decreasing the infiltration rate for clay, one can get more number of peaks. The sensitivity of other infiltration values was also required to be checked. After several trials of different values of seven parameters, it was clear that only by decreasing the infiltration values for silt, the peak has increased. It means by increasing these values, the peaks will be decreasing.

By keeping these observations in mind, 15 different trials were carried to attain the exact match in time series graph. The differences in base time period suggests the requirement to add base flow to surface runoff; which makes the base time period more. So, it could be derived that the runoff from the model does not account for base flow. By observing the topography of the catchment, it was very clear that there should be two streams. So

presence of many peaks as an output from the model could be due to time lag in both the surface runoff. Since the runoff in the field was measured only at the outlet, this reason seems to be logical.

By now, the following necessary requirements were:

i. There should be some guideline to choose the values for infiltration rate;
ii. The base flow and topography of the catchment should also be accounted for the further analysis;
iii. By incorporating above two points, a decision space should be fixed, in which the optimum values of parameters can be searched;
iv. While searching the parameters in decision space, there should be some objective function to attain.

5.3.2 Data of 96 Set 2

The infiltration rates for clay, silt and silty clay were investigated from the literature. In most of the cases, it was observed that the K_f and the Maximum infiltration values for silty clay and silt are approximately same, and it is half of that corresponding to clay. The maximum infiltration values were chosen 10 % more than the infiltration rate. So, for further studies, following relationship was finalised.

Type of soil	K_f (mm/hr)	Maximum Infiltration (mm/hr)	K_{st}
Silt clay	a1	1.1a1	
Silt	a1	1.1a1	5.0
Clay	0.5a1	0.55a1	

With the help of the above relationships, one needs to choose only one value of a1 and accordingly other values would change. Twenty different trials were carried out to fix the K_{st} values. The chosen K_{st} values varied from 0.5 to 10.0. It was observed that there is no change in time series graph for the K_{st} values from 0.5 to 4.0; the significant changes were recorded only for the K_{st} values 4.0 to 10.0. The RMSE was minimum for the K_{st} value 5.0. It was decided to fix K_{st} as 5.0 for the further analysis.

For each combination RMSE and NSE were calculated. Fifty different trials were carried out for the data set having period 12:00 on 26/8/96 to 00:00 on 17/9/96. The infiltration values started from 0.15 mm/hr and increased to 7.50 mm/hr at an interval of 0.15. The minimum RMSE and NSE were observed for the combination of values as shown below. The time series graph for these values of parameters is as shown in Figure 5.5.

K_f (mm/hr)	Maximum Infiltration (mm/hr)	K_{st}
5.10	5.61	
5.10	5.61	5.0
2.55	2.81	

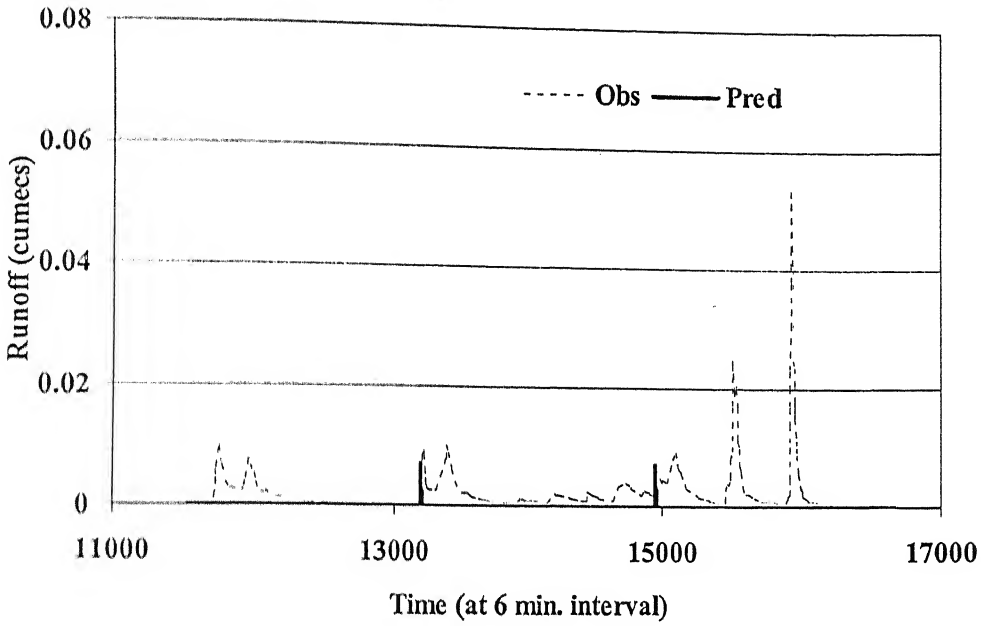

Figure 5.5: Time series plot corresponding to minimum error statistics

By observing the time series graph for all the trials, the best match in observed and predicted runoff was observed for the following combination.

K_f (mm/hr)	Maximum Infiltration (mm/hr)	K_{st}
1.05	1.15	
1.05	1.15	5.0
0.53	0.58	

The time series graph for this combination is as shown in Figure 5.6. In order to find out the reason for the higher peak values, the rainfall was also plotted on the same sheet. The peaks obtained from model were very logical. Whenever there is maximum rain or consecutive rains, the peaks were present. Similar was the case with observed data. The

peaks were too high and number of peaks was nearly same. The base time period was less in the case of predicted runoff.

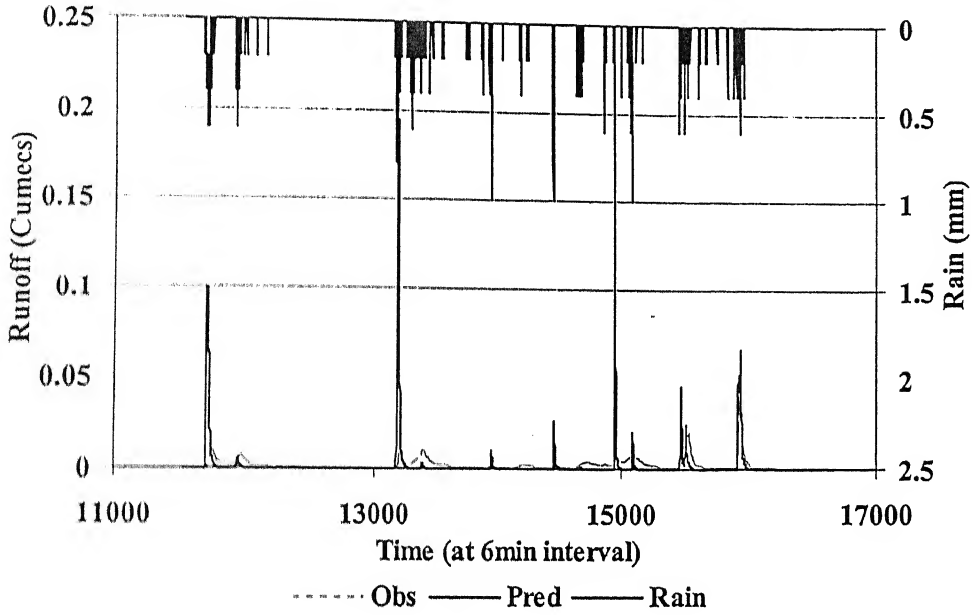

Figure 5.6: Best observed match in time series plot for 96 set 2

The variation of RMSE with the increase in K_f values are presented in Figure 5.7. The RMSE is an absolute measure of the residual variance from the developed model

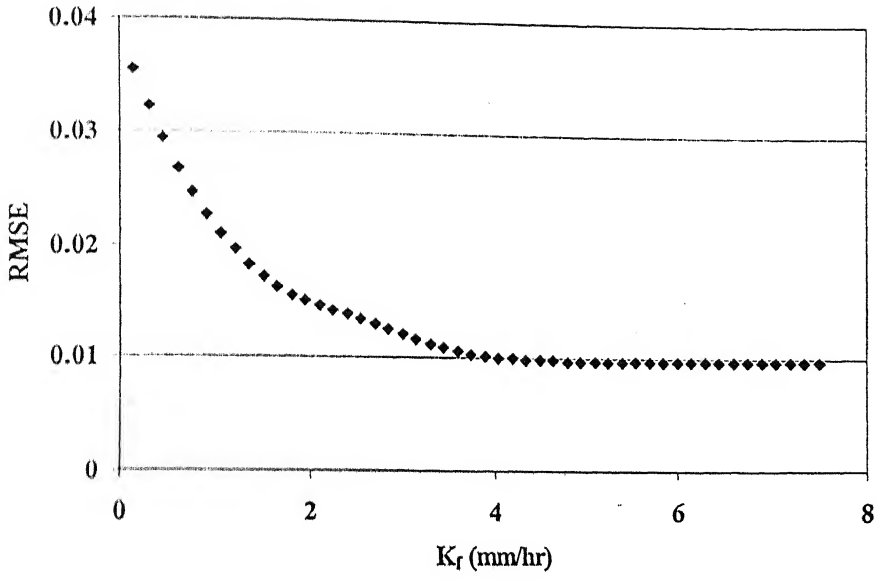

Figure 5.7: Variation of RMSE with increase in K_f values

To decrease the peak values and to get rid of number of peaks, the maximum infiltration rate was increased. Thirty trials were carried out by increasing the values from 10% to 4000% with respect to infiltration values. For each case, RMSE and NSE were calculated. The variations of RMSE and NSE with the increase in maximum infiltration values are shown in Figure 5.8. It followed the expected behaviour to reduce the peak values by increasing maximum infiltration rates. After increment of 800%, peaks started disappearing. MBE was also calculated. The variation of MBE with the increase in Maximum infiltration values is shown in Figure 5.9.

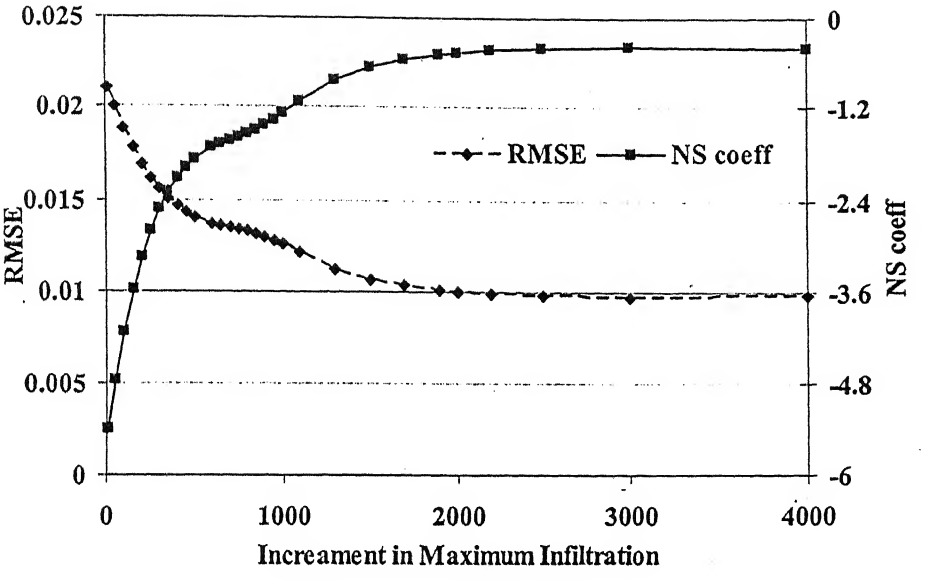

Figure 5.8: Variation in RMSE and NSC with increase in maximum infiltration values

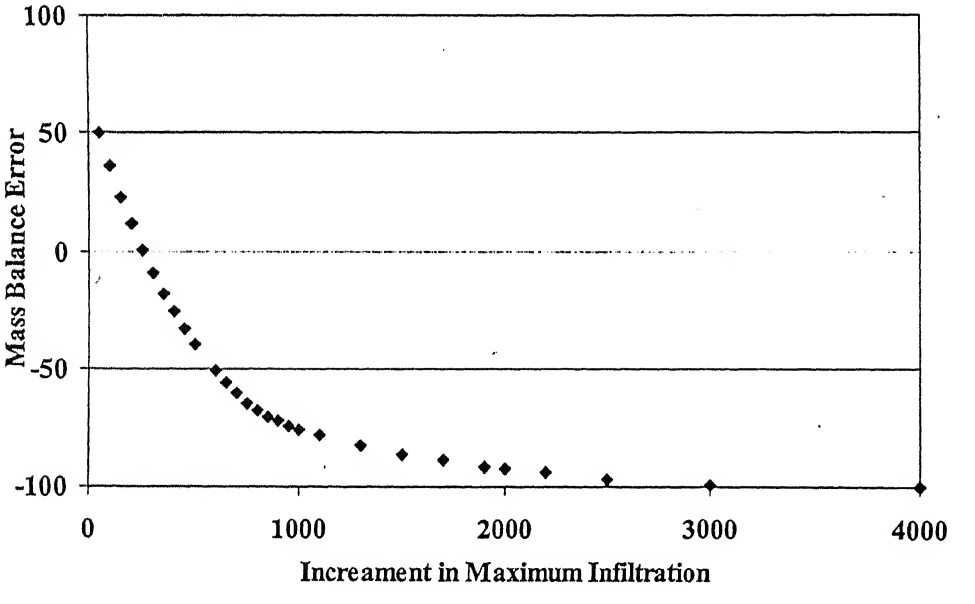

Figure 5.9: Variation in MBE with increase in Maximum infiltration values

5.4 Final 1996 trial

The observed ground runoff were available for 10 months period (8.2.96 to 31.12.96). Using this data set, the runoff for 6 minute interval was generated. The runoff values were assumed to be uniform for the period in which data were missing. On the basis of previous discussion, the range of each variable was decided as follows:

$20 \leq$ Maximum infiltration < 40mm/hr

$0.5 \leq K_f < 50$mm/hr

$3 \leq K_{st} < 10$

Using these ranges, now a decision space has been generated. Sixty different trials were performed by moving points on each face of the cube. The time period for this study was from 00:00 on 13/8/96 to 12:30 on 31/12/96. But results obtained from this study were not encouraging. So, the physics involved in each layer were studied to control the flow.

5.4.1 Physics involved in soil moisture modelling

The processes considered while developing WBM model needs to be understood to carry out further calibration trials. The entire processes are represented in Figure 5.10. The diagram is self explanatory. Deep percolation contributes to ground water which appears in channel, but the fate of deep percolation is not considered for the present study.

The significance of K_f and maximum infiltration values can be understood from Figure 5.11. By defining K_f and maximum infiltration values as an input to model, the infiltration curve is developed by using well defined equations within the model. For a given soil moisture, the infiltration and percolation rates are calculated from the developed graph. At this point, it is important to note that this graph is developed only for the 1st layer. In present study, the soil is of 3 different types. So, out of 6 parameters used earlier to calibrate the model, only 3 are used now. It depends on which layer comes at the top. The model is instructed to use the saturated hydraulic conductivity and maximum infiltration values corresponding to the soil type, which exists at the top layer only. It is possible to shift the curve upward or downward by defining a factor. The K_f and maximum infiltration values will be multiplied by that factor and rest of the curve will be developed accordingly.

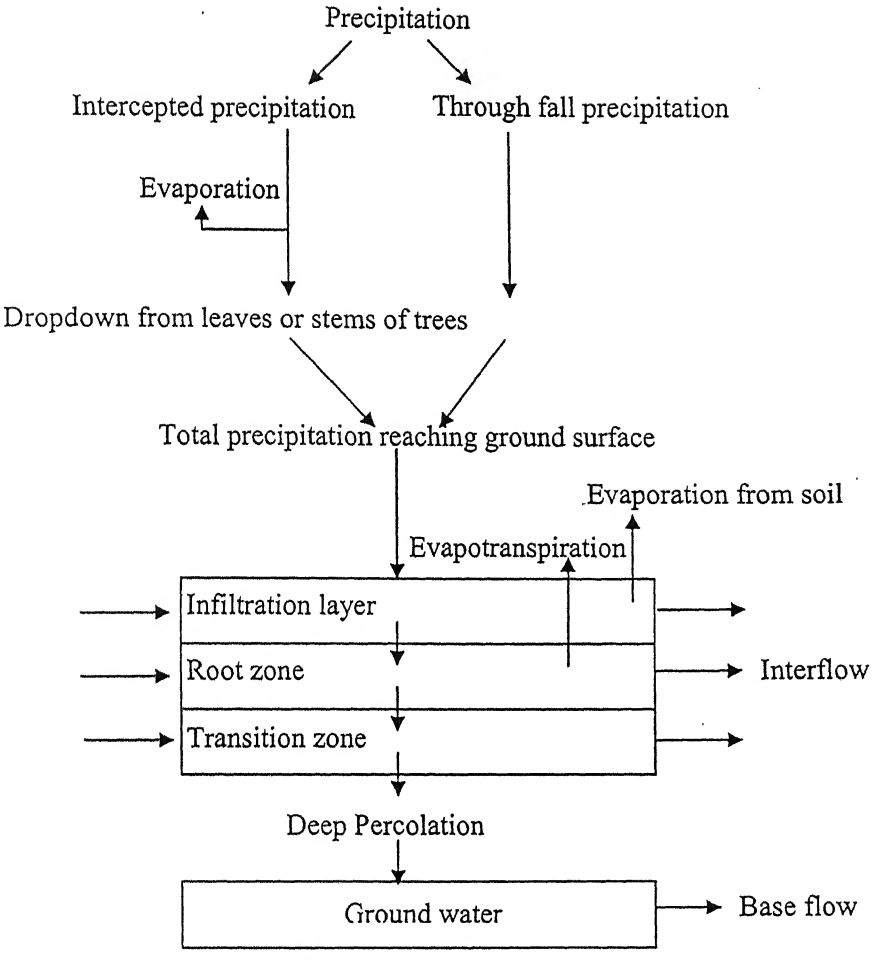

Figure 5.10: Processes considered in WBM model

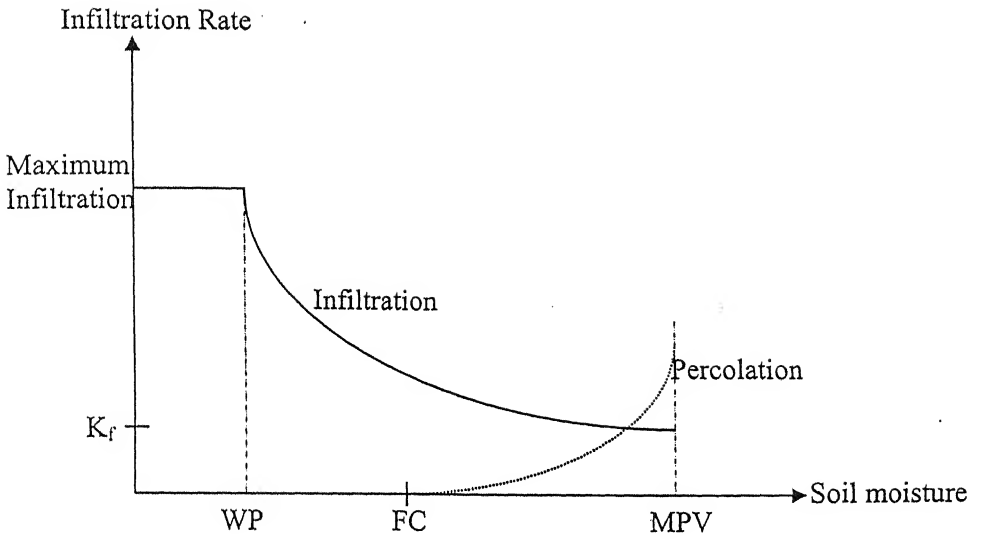

K_f: Saturated hydraulic conductivity, WP: Welting Point, FC: Field capacity, MPV: Maximum pore volume

Figure 5.11: Infiltration and percolation curve

After realizing these facts, the following were decided to be checked for next calibration trials.

i. Observe soil moisture profile besides time series graphs
ii. Check the sensitivity of factor to be used
iii. Significance of interflow should also be observed.

Fifty different trials were carried out by changing the factor from 1 to 50. The factor of 4.0 showed better results. For these trials, the Kf and maximum infiltration values were kept as mentioned below:

K_f (mm/hr)	Maximum Infiltration (mm/hr)
1.05	1.15
1.05	1.15
0.53	0.58

So, by defining a factor of 4.0, all the values will be multiplied by 4.0. Hence, it again showed values close to the best combinations decided since beginning (shown below) except the infiltration values for clay.

Kf(mm/hr)	Maximum Infiltration (mm/hr)
4.5	4.6
4.5	4.6
0.05	0.06

It was observed that by increasing this factor, runoff increases. It was against the expectation that the runoff will decrease by increasing the K_f and maximum infiltration rate. One of the possible reasons could be back water effect. But since the ground water flow has not been considered for this study, so this reason does not seem logical. To include the effect of interflow, a channel of 5 m long was introduced artificially in the catchment at the last grid cell near to the outlet. This helps interflow to be added to the surface runoff.

5.4.2 Discussion on surface runoff and soil moisture profile

It was decided to consider small duration for model run and investigate the output results in detail. The duration considered was from 12:00 on 26/8/96 to 23:54 on 30/9/96. The time series graph obtained is shown in Figure 5.12. The conclusions out of discussion in section 5.4.1 were fully incorporated during these model runs. It is clear from time series graph that except the presence of one high peak, other peaks are almost matching for observed and predicted data. The problem of presence of such high peaks from predicted runoff values from model exists since beginning of calibration trials. So, at this juncture, it was felt that there could be error in observed ground data. It was urgent need to contact the concerned person who was directly involved during data collection. Dr. Andrew Western (the data were downloaded from his homepage) referred some publications which discuss such difficulty in developing model using available data for Tarrawarra catchment.

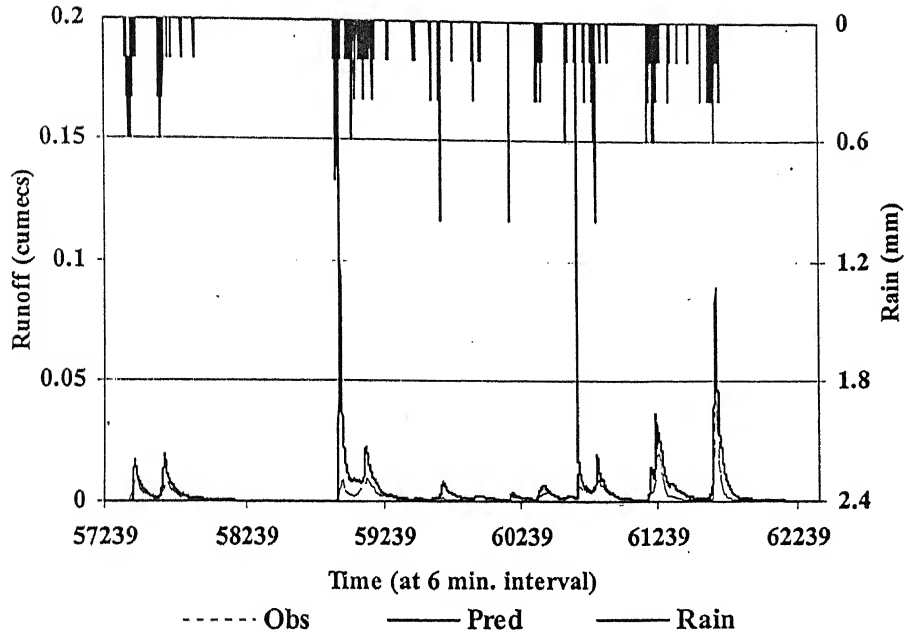

Figure 5.12: Time series plot obtained from final trial

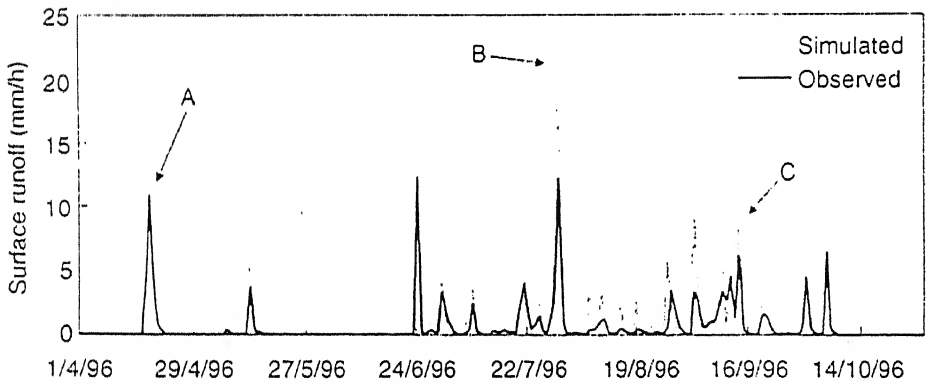

Figure 5.13: Time series plot obtained from literature

Western [2000] mentions that the annual surface runoff during 1996 is overestimated by 31% from the model developed by his research group. The time series hydrograph showing

these overestimations were collected from literature and is shown in Figure 5.13. By comparing the characteristics of hydrograph for the period 12:00 on 26/8/96 to 23:54 on 30/9/96, it also shows presence of many peaks which are higher than observed ground data.

The next target was to analyse soil moisture pattern. Soil moisture pattern measured in ground on different dates were collected from literature and is presented in Figure 5.14. Western [2000] mentions that there are some small scale features that are critical to the runoff response of the catchment. These are the narrow bands of high soil moisture along the drainage lines and the model should be able to capture these. It also mentions that during winter, the catchment soil moisture is very high and extensive areas are saturated. The high moisture values in drainage lines on September 2nd and 20th are likely to be slightly too high due to surface water ponding introducing some measurement errors. The soil moisture profile obtained from WBM model at 12:00 on 2/9/96 is shown in Figure 5.15. It is clear that the model is able to capture narrow bands of high soil moisture along the drainage lines. The remaining area with high value of soil moisture is due to approximations assumed during soil classifications in the catchment.

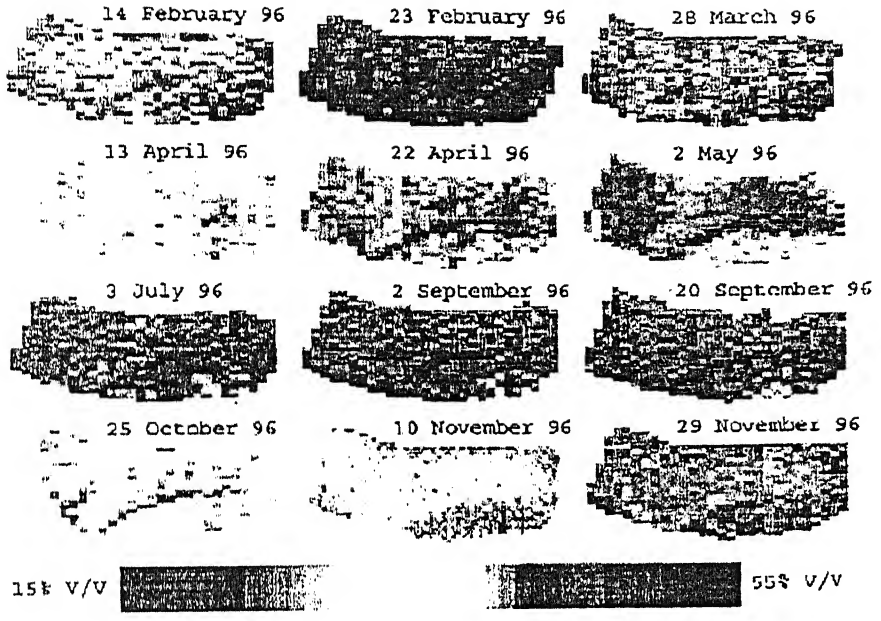

Figure 5.14: Soil moisture profile obtained from literature for Tarrawarra catchment

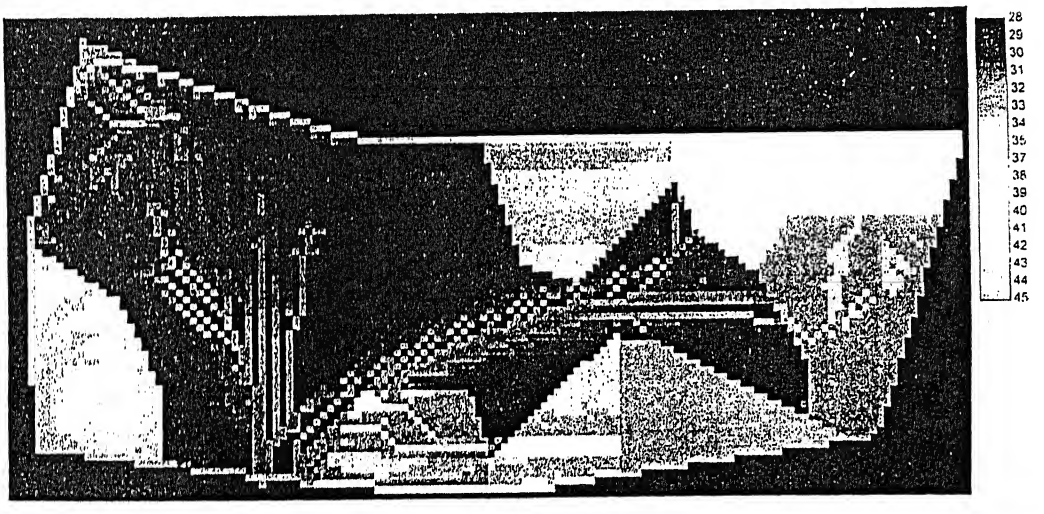

Figure 5.15: Soil moisture profile obtained from model

5.5 Calibration and validation using newly generated data set

Based on the experience obtained at TU Darmstadt, another trial was made to achieve better calibration by trial and error in a more systematic way. The data generation and selection of calibration and validation periods are explained in section 4.8. The procedure to calibrate the model was kept same as discussed stepwise in section 5.1. The model calibration was tried for Period 4L, 4M and 4H. By using the best combination of parameters obtained during calibration, the model was validated for period 2L, 2M and 2H (described in section 4.8). The set of parameters obtained and corresponding time series graph are presented below from Figure 5.16a to Figure 5.16f.

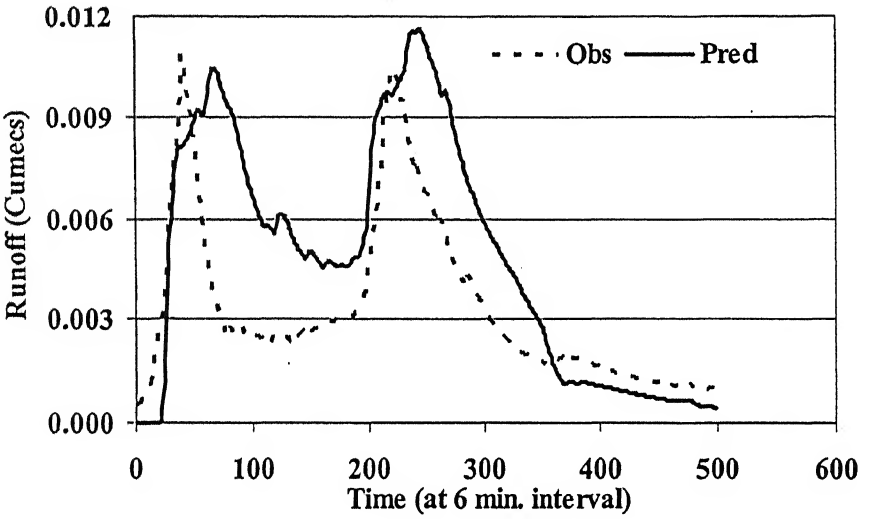

Figure 5.16a: Time series graph for calibration period of Low peak event i.e. period 4L

Combination of parameters for period 4L

K_f (mm/hr)	Maximum Infiltration (mm/hr)	K_{st}
6.5	7.1	
6.5	7.1	0.3
3.2	3.5	

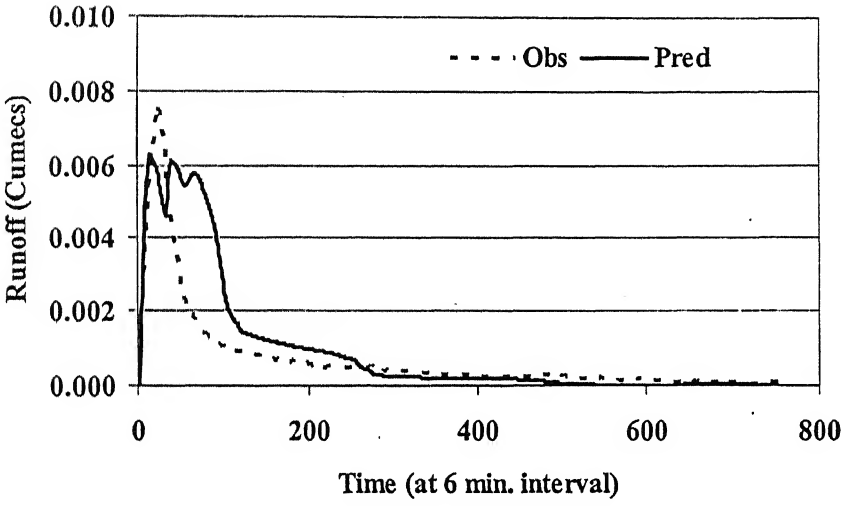

Figure 5.16b: Time series graph for validation period of Low peak event i.e. period 2L

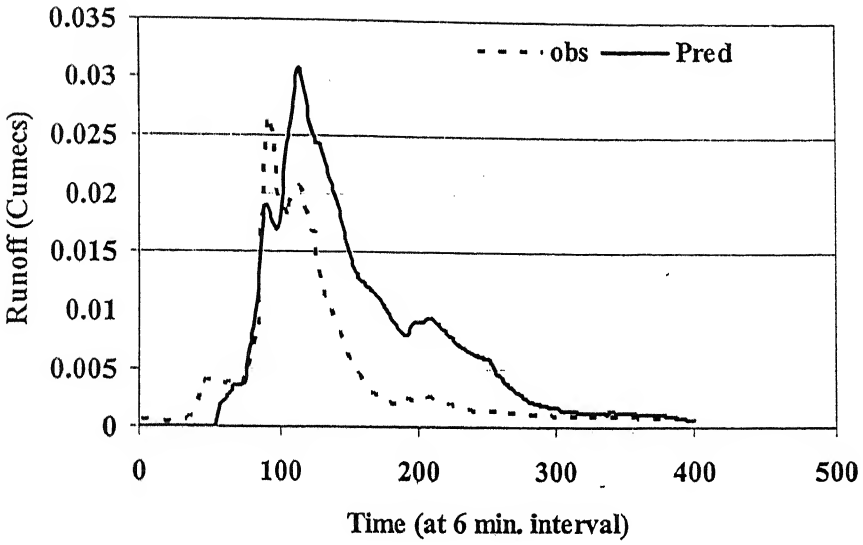

Figure 5.16c: Time series graph for calibration period of medium peak event i.e. period 4M

Combination of parameters for period 4M

K_f (mm/hr)	Maximum Infiltration (mm/hr)	K_{st}
4.5	4.6	
4.5	4.6	3.0
2.25	2.3	

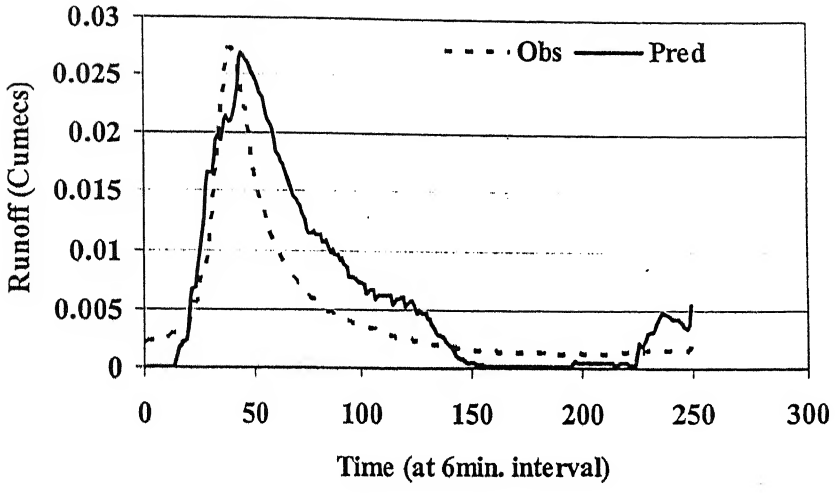

Figure 5.16d: Time series graph for validation period of Medium peak event i.e. period 2M

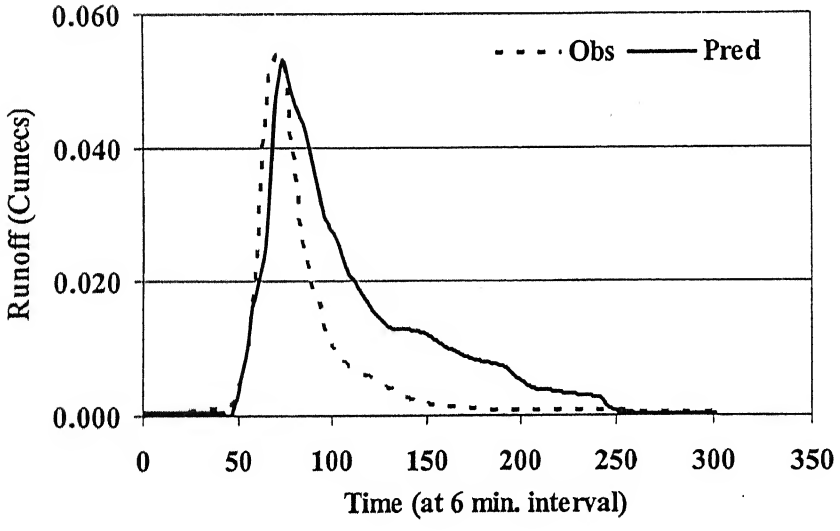

Figure 5.16c: Time series graph for calibration period of High peak event i.e. period 4H

Combination of parameters for period 4H

Kf(mm/hr)	Maximum Infiltration (mm/hr)	K_{st}
2.5	2.8	
2.5	2.8	5.0
1.3	1.4	

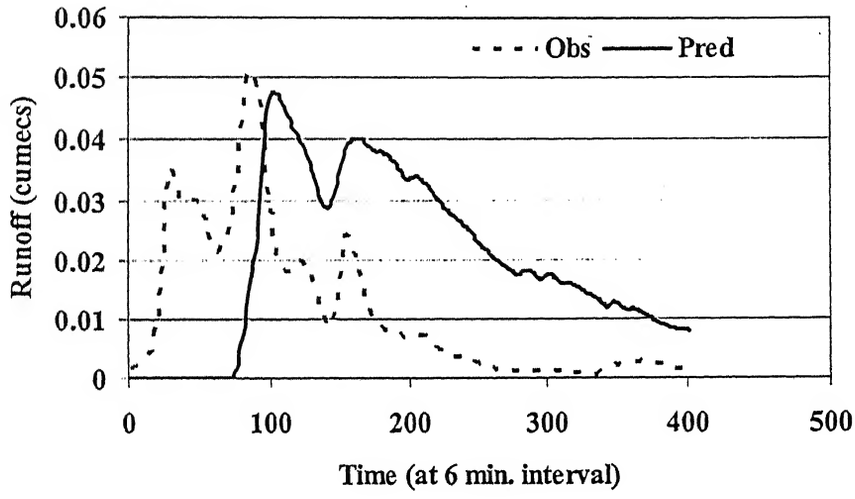

Figure 5.16f: Time series graph for validation period of High peak event i.e. period 2H

5.6 Results and discussion

The error statistics for calibration trials of different periods of year 1995 are presented in Table 5.2a. The date and time of these periods can be recalled from sections with same headings in this chapter. By looking at the errors, no definite pattern in any of the error

statistics are observed. Considering only R values suggests that 1995 trial – 1 with K_{st} of 3.0 provides the best combination of parameters out of all trials.

The error statistics obtained during calibration for data of different periods of year 1996 are presented in Table 5.2b. By looking at R values, it clearly indicates that the observed and predicted runoff are not matching. The AARE vaues are very high and other errors are also not considerable. However, only by visual interpretation of time series graph suggested best match in case of Final trial.

The error statistics for calibration (Period – 4) and validation (period – 2) periods for low, medium and high peak flow events are presented in Table 5.2c. It is clear that the RMSE is decreasing from calibration to validation except in case of high peak flow event. Similarly R, AARE and SSE also showing improvement from calibration to validation for low and medium peak flow events.

On the basis of time series graphs and error statistics obtained out of different calibration trials, reasonable results were obtained in case of 1995 trial – 1 with K_{st} of 3.0 and period 4M. The combination of parameters in both the cases were averaged and the resulting parameter values are presented below. As discussed earlier in section 5.3.2, literature suggests that the K_f and Maximum infiltration values for clay should be half of the same for silt clay.

	K_f(mm/hr)	Max. Inf. (mm/hr)	K_{st}
Silt clay	4.5	4.6	
Silt	4.5	4.6	3.0
Clay	1.175	1.18	

As discussed earlier in section 5.3.2, literature suggests that the K_f and Maximum infiltration values for clay should be half of the same for silt clay. By keeping this logic in mind the final best combination of parameters were declared as presented below.

	K_f (mm/hr)	Maximum Infiltration (mm/hr)	K_{st}
Silt clay	4.5	4.6	
Silt	4.5	4.6	3.0
Clay	2.25	2.3	

Table 5.2a: Error statistics of different calibration trials for 1995

Period	RMSE	NRMSE	NSE	E1	R	AARE	SSE
1995 Trial -1, kst of 1.0	0.000375	2.973	-0.024	0.204	0.045	87.13	0.000065
1995 Trial-1, kst of 3.0	0.000113	0.893	0.908	0.453	0.945	91.40	0.000006
1995 Trial -1, kst of 5.0	0.000934	7.406	-5.35	-0.555	0.869	103.26	0.000406
1995 Trial – 1, kst of 9.0	0.000137	10.896	-12.75	-1.374	0.72	123.58	0.000878
1995 Trial-2	0.0039810	1.269	-1.458	-0.258	0.0001	135.8	0.003169

Table 5.2b: Error statistics of different calibration trials for 1996

96 set 1	0.002437	2.706	-0.045	0.308	0.247	98.36	0.000743
96 set 2	0.021042	4.065	-5.397	-0.473	0.122	335.48	0.12930
Final trial	0.014730	3.710	-3.010	-0.323	0.437	650.39	0.08806

Table 5.2c: Error statistics of different calibration and validation for 1996

4L	0.002678	0.794	-0.192	-0.099	0.627	71.15	0.003586
2L	0.000995	1.3715	0.396	0.307	0.686	68.67	0.00075
4M	0.005	1.189	0.293	0.1302	0.719	125.04	0.01
2M	0.00375	0.77	0.6198	0.301	0.805	83.175	0.003502
4H	0.00786	1.243	0.595	0.3099	0.742	215.54	0.01857
2H	0.0209	1.823	-1.741	-0.842	0.0001	496.32	0.1745

In the next chapter, the selected combination of parameter has been used to check the sensitivity of dynamic land use parameters.

Chapter 6

Sensitivity analysis of dynamic land use parameters

6.1 General

In this chapter, first the different dynamic land use parameters have been briefly introduced. The seasonal variation of root depth, vegetation cover (BG), and leaf area index (LAI) were available for different type of forests. By applying the seasonal variations, the sensitivity of the parameters in terms of water balance have been observed.

6.2 Dynamic land use

Land use is based upon the function of land, i.e. the purpose for which the land is being used. A given land use may take place on one, or more than one pieces of land and several land uses may occur on the same piece of land. The word dynamic is added to stress upon the variations as a function of time e.g. seasonal cycle of vegetation and changes by introducing unproductive lands and vegetation of different types over the year.

The catchment considered in the present study is covered of grass only and is used as pasteur land. The abovementioned land uses have been applied artificially. In the WBM, it is possible to alter the following parameters:

i. Root depth

ii. Percentage of Vegetation cover (BG) and its seasonal cycle

iii. Leaf area index (LAI) and its seasonal cycle

iv. Unproductive land

v. Roughness.

The parameters are briefly described here. These informations are collected from Gurtz [2004].

The root depth

The root depth is defined as the vertical distance form soil surface up to which 95% of all plant roots are found. Root growth is very sensitive to climate change and soil properties (especially moisture), so it is very important to properly quantify interaction between the climate, soil and plants. The soil moisture content available for evapotranspiration is controlled by the actual saturation of the soil and by the structure of the soil's root zone.

Leaf area index and vegetation density

The seasonal cycle of vegetated surfaces can be well described through two seasonally varying parameters: The leaf area index (LAI) and the density of vegetation. In this way, it is possible to capture the different periodical behavior of the different classes of vegetation. LAI is the total area of leaves in relationship to the ground below them.

LAI describes a fundamental property of the plant canopy and its interaction with the atmosphere. Various soil – vegetation atmosphere models and hydrological models use LAI. The main hydrological processes related to seasonal development of these vegetation specific parameters are interception and evapotranspiration. Higher LAI means higher water storage capacity on leaves, which determine a higher potential for interception evaporation in the seasons with higher LAI.

The surface roughness

The average height of the different types of vegetation is assumed as index for the surface roughness. Roughness is used to calculate wind effects on evapotranspiration, which affects the rate of moisture transfer from the vegetation to the atmosphere. Hence, atmospheric and hydrological models require accurate estimates of surface roughness. By changing the values of these parameters, one can simulate different type of vegetation, their characteristics throughout the year and unproductive land. These parameters are linked to several processes of the hydrological cycle. These land uses alter the land in different ways. In terms of the movement of water in the basin, land use often changes the permeability of the land surface, thus affecting surface drainage systems and natural hydrology. Land use is important to the development of long term forecasts to guide present development. Systematic decision making regarding appropriate land uses for different parts of a watershed system has a central role in projecting or impacting valued landscapes.

6.3 Sensitivity of parameters for grass

The effect of changes in root depth, BG, LAI and percentage coverage of unproductive land on water balance was observed for the period 00:00 on 30.03.96 to 23:54 on 30.12.96.

6.3.1 Changes in root depth

The root depth was varied from 0.45 mm to 0.8 mm. The graph showing the effect is presented in Figure 6.1. The precipitation is divided into through rainfall (TR), interception evaporation (IE), soil evaporation (SE), transpiration (T) and evapotranspiration (EPT). From Figure 6.1, it is clear that there is no effect in through rainfall, interception, and soil evaporation with the change in root depth. Transpiration and evapotranspiration values change by increasing root depth from 0.45 m to 0.7 m. In this case, BG was assumed to be 85 with LAI of 1.7 and K_{st} value was fixed as 3.0.

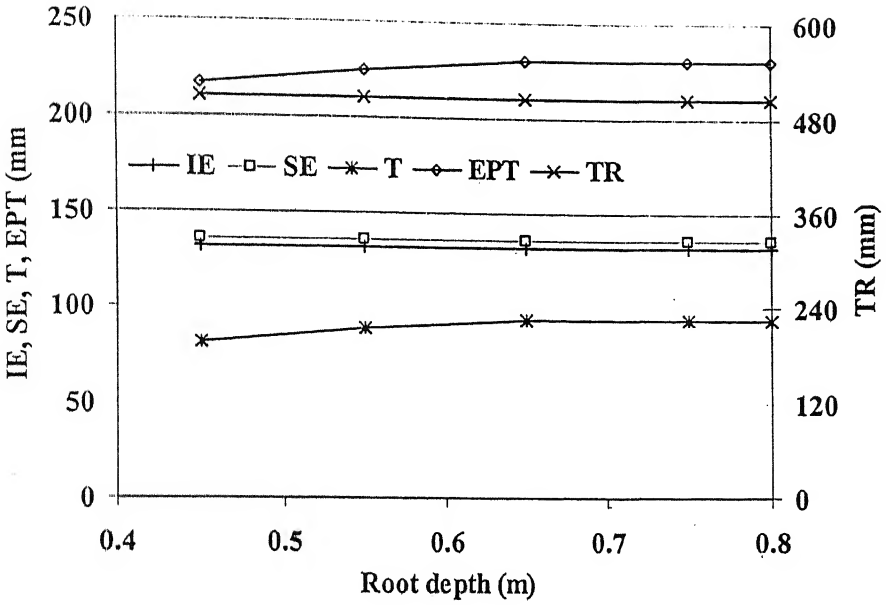

Figure 6.1: Effect of changes in root depth

The transpiration increases with an increase in the root depth up to 0.75 m. The maximum depth of soil considered in the present study is only 0.75 m. So, this might be the reason of constant transpiration value by increasing the root depth beyond maximum possible soil thickness.

6.3.2 Changes in vegetation cover

The change in water balance was observed for BG varying from 20 to 100. In this case, LAI was kept constant at 1.7. The effects are presented in Figure 6.2.. By increasing vegetation cover over the catchment, TR was decreasing because now a part of rain will be intercepted by leaves as expected. Hence, IE has increased. Since rain reaching ground

surface decreases with an increase in the BG; so SE is decreasing. The amount of T is increasing because of presence of large number of trees in the catchment.

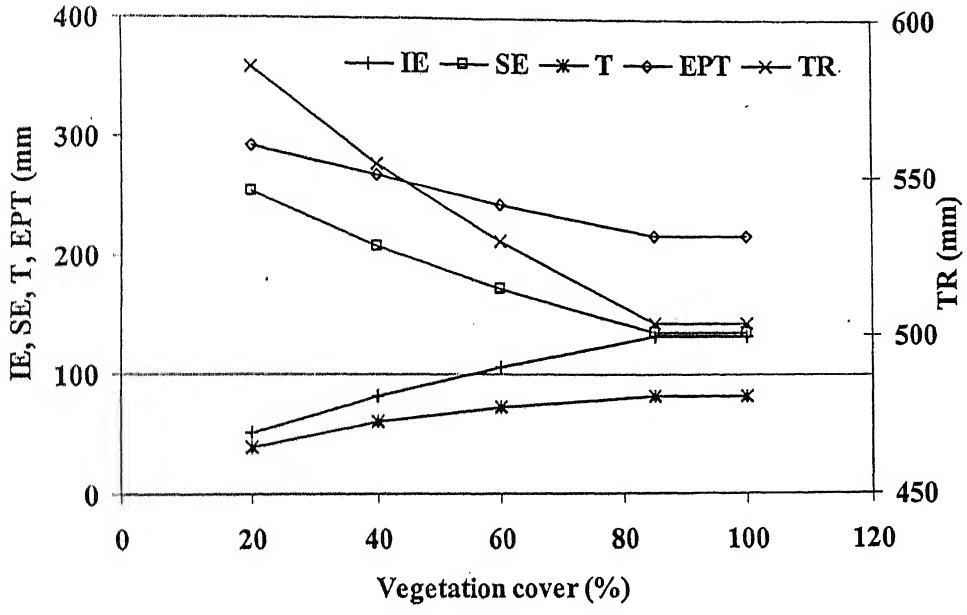

Figure 6.2: Effect of changes in BG

6.3.3 Changes in leaf area index

LAI were varied from 1.0 to 10.0. The effect on water balance is shown in Figure 6.3. TR, SE and EPT values are decreasing while IE and T values are increasing with the increase in LAI values. This looks very realistic that increment in LAI resulted into large obstruction in amount of rain reaching to ground and hence high IE. T is increasing due to presence of healthy or vegetated trees fully covered with leaves.

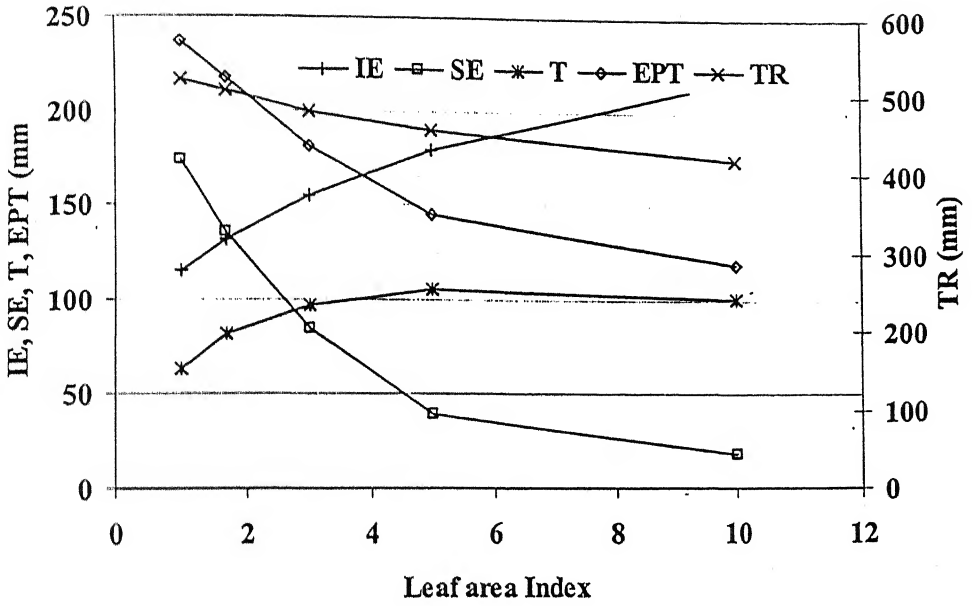

Figure 6.3: Effect of changes in LAI

6.3.4 Changes in unproductive land

For this study, the root depth, BG and LAI values were 0.45 mm, 85 and 1.7, respectively. The percentage of unproductive land in earlier cases was kept at 0. At this point, it is necessary to clearly define the meaning of percentage of unproductive land along with percentage of vegetation cover. In the WBM model, it is necessary to define ID corresponding to a part of the catchment. One can divide the catchment into two or more parts or it can be of single type only. By defining type, it means that the characteristics in terms of root depth, vegetation cover and LAI will be same for that portion of the catchment. These parameters are assigned to a single pixel and in case of single type of catchment, same characteristics is assigned to all the pixels of the catchment.

The partition within a single pixel can be well described using Figure 6.4. Initially the pixel is of uniform characteristics. By defining a% of vegetation and b% of unproductive land, movement of water in a% of pixel will be slow due to presence of vegetation. The movement of water in b% of the rest (100-a) will be fast because in this portion, water is allowed to move horizontally not vertically. In the rest part of the pixel, the water movement will be normal.

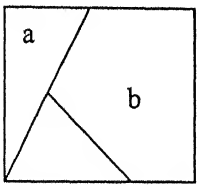

Figure 6.4: Partition of a pixel according to land use

For the present study, the percentage unproductive land was varying from 20% to 100% by keeping vegetation cover at 85% and single type to the whole catchment. The changes in water balance have been presented in Figure 6.5. The amount of IE, T and EPT has decreased by increasing percentage of unproductive land. Through rainfall is increasing, because obstruction by leaves is decreasing. By increasing percentage of unproductive land within the catchment, automatically vegetated covered area is decreasing and hence in case of 100% unproductive land, there is no IE, SE, T and EPT.

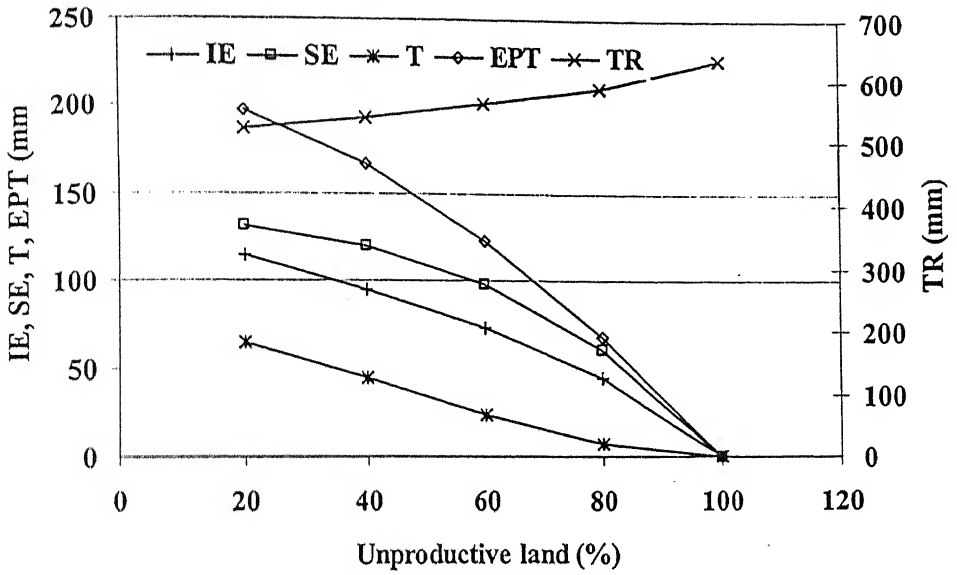

Figure 6.5: Effect of introduction of unproductive land

6.4 Different Land uses

To observe the effect of different dynamic land use changes, 6 different types of forests were artificially generated in the catchment. Those are Young coniferous forest (NW1), Old coniferous forest (NW2), Young deciduous forest (LW1), Old deciduous forest (LW2), Young mixed forest (MW1), Old mixed forest (MW2).

For each forest, two subcategories were generated to run the model. When BG is kept constant throughout the year and only seasonal variations of LAI is considered (denoted by 'a') and when seasonal variations of both BG as well as LAI is considered (denoted by 'b').

variations but there was no variation in BG as observed from Table 6.2. This resulted into small changes in transpiration values only.

Table 6.2: Seasonal variations for coniferous forest

Type		Jan	Feb	Mar	Apr	May	Jun	Jul	Aug	Sept	Oct	Nov	Dec	Avg
NW1	BG	85	85	85	85	85	85	85	85	85	85	85	85	85
NW1	LAI	6.0	6.0	6.0	6.0	6.0	6.0	6.0	6.0	6.0	6.0	6.0	6.0	6.0
NW2	BG	90	90	90	90	90	90	90	90	90	90	90	90	90
NW2	LAI	10	10	10	10.2	10.5	10.8	11	11	11	11	11	10.5	10.5

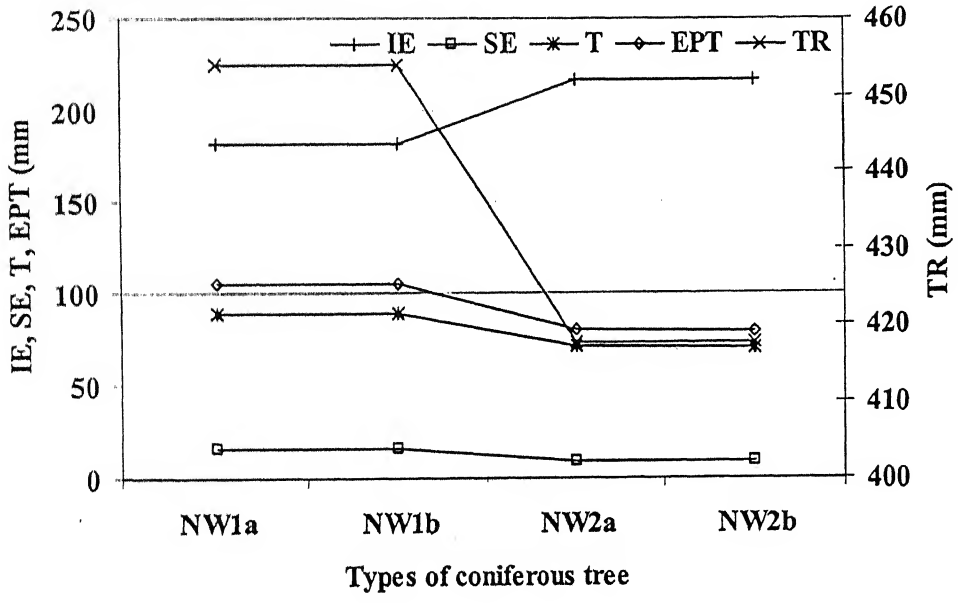

Figure 6.6: Cumulative values of different components of rain for coniferous forest

By comparing values from the graphs for young and old coniferous trees, it is cleat that TR, SE, T and EPT has decreased while IE has increased. This might have resulted due to high value of average LAI and BG in case of old coniferous tress. Time series graphs were

drawn for all the four cases (NW1a, NW1b, NW2a, and NW2b). No definite conclusions could be drawn using these graphs. By manual observations, it was found that the variations were very small in all the components for different periods.

6.4.1.2 Deciduous forest

The LAI and BG for deciduous forests have much variation with season. The values are presented in Table 6.3. In winter, it has LAI of 0 and in the summer seasons, it goes up to 2.5. The BG for deciduous forest in winter is 10 for young trees and 15 for old trees, while in summer it reaches 60 for young trees and 70 for old trees. The cumulative values of different components of rain obtained from model are presented in Figure 6.7.

Table 6.3: Seasonal variation for deciduous forest

Type		Jan	Feb	Mar	Apr	May	Jun	Jul	Aug	Sept	Oct	Nov	Dec	Avg
LW1	BG	10	10	10	20	60	60	60	60	50	30	10	10	32.5
LW1	LAI	0	0	0	0.5	2.0	2.5	2.5	2.5	2.5	0.5	0	0	1.0
LW2	BG	15	15	15	25	70	70	70	70	60	40	15	15	40
LW2	LAI	0	0	0	1	3	3.5	3.5	3.5	3.5	1.0	0	0	1.6

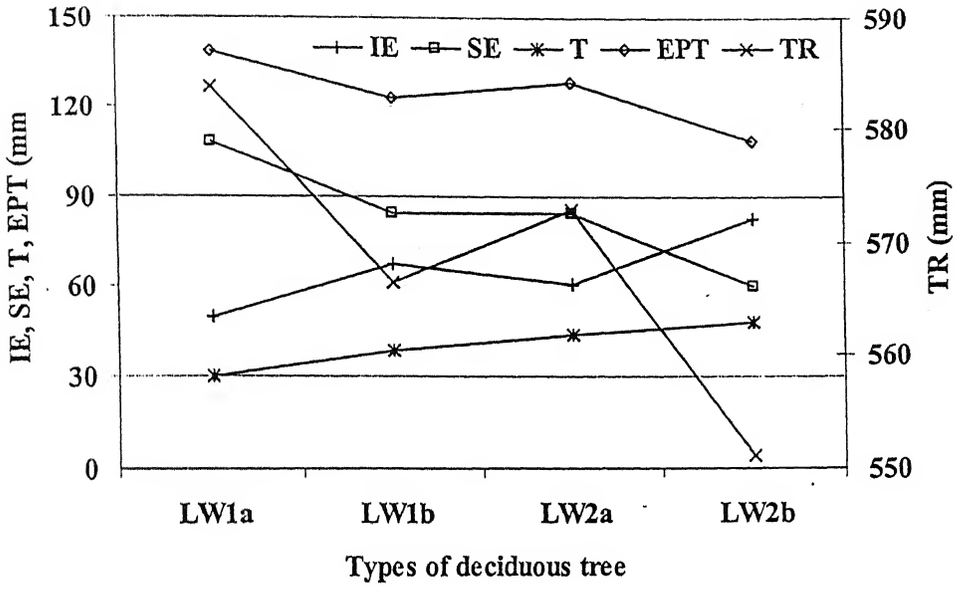

Figure 6.7: Cumulative values of different components of rain for deciduous forest

By comparing LW1a and LW1b, it was observed that TR, SE and EPT has decreased while IE and T has increased. Average values of BG is kept constant as 32.5 for LW1a. By introducing the seasonal variations of BG in case of LW1b, the decrement in through rainfall and EPT is obvious, because during the summer seasons, BG goes as high as 60 and hence increment in IE. Similar pattern has been observed for LW2a and LW2b, which can be explained with similar logic.

6.4.1.3 Mixed forest

The seasonal variations in LAI and BG for mixed forest are presented in Table 6.4 are nearly average of those for coniferous and deciduous forest. In winter season, the LAI for young and old trees is 1.4 and 2.0 respectively. In summer, for young trees it increases to

4.0 and for old trees it goes up to 5.54. The cumulative values of different components of rain for mixed forest are shown in Figure 6.10.

Table 6.4: Seasonal variations for mixed forest

Type		Jan	Feb	Mar	Apr	May	Jun	Jul	Aug	Sept	Oct	Nov	Dec	Avg
MW1	BG	42	42	42	55	65	65	65	65	55	45	42	42	52
MW1	LAI	1.4	1.4	1.4	1.7	2.5	4	4	4	4	2.5	1.7	1.4	2.5
MW2	BG	46	46	46	60	80	80	80	80	65	48	46	46	60
MW2	LAI	2	2	2	2.5	4.2	5.54	5.54	5.54	5.54	4.2	2.2	2.0	3.6

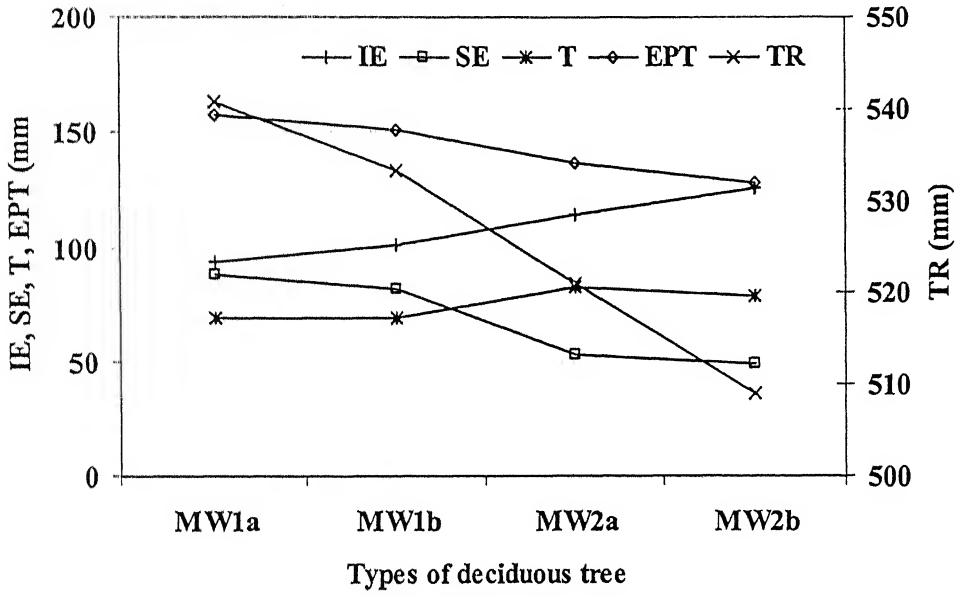

Figure 6.10: Cumulative values of different components of rain for mixed forest

By comparing values for MW1a and MW1b, it is clear that TR, SE, and EPT values are decreasing while IE and T are increasing. Similar is the case for MW2a and MW2b except

T has decreased in this case. From Table 6.4, it is clear that the BG is high in summer seasons. So, when variation in BG was considered, this resulted into increase in values of IE and T.

Chapter 7

Summary and conclusions

7.1 Summary

This thesis presents the findings of a study carried out with the purpose of using hydrologic models to check the sensitivity of dynamic land use parameters in a catchment. Many distributed hydrologic models were explored in an attempt to understand the use of RS and GIS in hydrological applications.

The WBM model was used to carry out the distributed hydrologic modelling in this study. The climatic and hydrologic data of Tarrawarra catchment, Australia were used to apply WBM model. The available metereological data were processed to generate input files required to run the model. A method of trial and error was employed to estimate the seven parameters of the WBM model. The time series graphs between observed and predicted runoff and certain error statistics were used to check the accuracy of calibration. Based on various trials using data of different periods, a combination of parameters was selected for which there was good match in time series graph and errors were also encouraging.

After fixing the parameters, the sensitivity of dynamic land use parameters were analysed. The seasonal change in root depth, percentage of vegetation cover in the catchment and leaf area index of the plant was considered as dynamic land use

parameters. Initially, the sensitivity of these parameters was checked for the catchment uniformly covered with grass. In this case, the seasonal variations were not accounted. Later, the change in water balance was observed by using seasonal variations of the land use parameters for coniferous, deciduous and mixed forest.

7.2 Conclusions

The results obtained during calibration of the WBM demonstrate that the WBM is able to capture the complex and non-linear relationship of rainfall runoff processes by taking into account the topography and spatial heterogeneity of soil type and land use. It is found that the model is sensitive to mainly seven parameters which change the model performance significantly. Moreover, the roughness is the most sensitive parameter. The non-uniform behaviour of infiltration rate with soil moisture played a major role in generating the response of the model. This created difficulty in estimating the values of parameters in the trial and error procedure. The time series graph and error statistics can only be able to demonstrate the direction to choose the values of parameters. It is unable to provide insights into the complex relationships. The findings of calibration presented in this report are only based on the evaluations of surface runoff. Due to discontinuity in available data, the soil moisture patterns could not be evaluated always except for a few occasions.

The results of the sensitivity analysis of dynamic land use parameters show that the spatially distributed hydrologic model is a good tool to assess the hydrological change due to land use changes. GIS appears to be an efficient tool for presentation of seasonal variations of these parameters. Introduction of different types of vegetation in

the catchment affects the water balance. This study clearly demonstrates that interactive integration of spatial data and application of distributed hydrologic model in GIS environment provides a powerful tool for assessment of effects due to land use changes. Future changes in land use can also be incorporated in the model. Thus land use planning and management can be done efficiently. Based on the changes in different components of hydrologic cycle, it is concluded that the percentage change in water balance due to introduction of mixed forest lies almost at the middle of the changes observed due to coniferous forest and deciduous forest.

7.2 Scope for future work

No study is complete in itself, and there is always scope of its improvements. It is important to note that the primary analysis of the highly detailed data set is a critical stage in generating hydrologic models. In the present study, the periods used in the model were decided based on continuously available data set. It is required to fix the continuous 6 min. data set for at least one full year. This could be done by close observation of the pattern in the data set and accordingly fill the missing data.

The evapotranspiration flux is one of the most significant fluxes in hydrologic modeling. In the present study, modified Penman-Monteith equation has been used to calculate evapotranspiration for 6 min interval. In most of the cases, the Penman-Monteith equation is used to find out daily evapotranspiration. So, the validity of the modified formula needs to be checked.

At some occasion, the unavailable surface runoff values were generated by proper interpolation. For the surface runoff data measurement, water levels in the flume were measured every minute and were saved when the changes in water level exceed 1.5 mm. This means that the missing data could be assumed as constant. Such methods may lead to errors in data that becomes limitation of the whole study.

Use of optimisation algorithms to search the optimum values of saturated hydraulic conductivities can improve the model performance and needs to be investigated. In doing so, defining objective function is a major issue. By literature review and by gaining personal experience by assigning different error statistics as an objective function could lead to suitable objective function. Before defining constraints for optimisation problem, a detailed sensitivity analysis to find out possible optimal region is necessary. The studies presented in Duan (1992), Yapo (1998), Madson (2003) and Madson (2000) can provide necessary guideline in this direction.

For the complete analysis of the effects of land use changes in the catchment, it is important to introduce urbanised area also to make it realistic urban development. This could be done by partitioning the catchment into different groups and then assigning different land uses for each group. This analysis will exactly simulate the establishment of buildings, trees and other land uses and its effect on future water availability inside and in surrounding area of the catchment.

It would probably lead to improved calibration, if one were to calibrate the model against the soil moisture patterns and then use the model to predict runoff. Available

soil moisture patterns at key points in time could be used to estimate the field capacity and welting point.

References

Abbott, M. B., Bathurst, J. C., Cunge, J. A., O'Connell, P. E., and Rasmussen, J. (1986a). ''An introduction to the European Hydrologic System-Systeme Hydrologique Europeen, SHE, 1: History and philosophy of a physically-based, distributed modeling system.'' *J. Hydrol.,* 87, 45–59.

Abbott, M. B., Bathurst, J. C., Cunge, J. A., O'Connell, P. E., and Rasmussen, J. (1986b). ''An introduction to the European Hydrologic System-Systeme Hydrologique Europeen, SHE, 2: Structure of a physically-based, distributed modeling system.'' *J. Hydrol.,* 87, 61–77.

Aerts, J. C. J. H., Kriek, M. and Schepel M. (1998). "STREAM (Spatial tools for River basin and Environment and Analysis of Management options): 'set up and Requirements'." Phys. Chem.. Earth (B), Vol. 24, No. 6, 591-595.

Aerts, J.C.J.H., & Bouwer, L.M. (2002). STREAM Krishna - a hydrological model for the Krishna River in India. IVM-report (E-02/12), Institute for Environmental Studies, Amsterdam, 34.

Bastidas, L. A., Gupta. V. H. and Sorooshian, S. (2002). "Chapter 2: Emerging paradigms in the calibration of hydrologic models." *Mathematical models of large watershed hydrology*, V. P. Singh and D. K. Fervert, eds., Water resources publication.

Baungartner M, Schultz G. A. and Johnson A. I. (1997), *Remote Sensing and GIS for Design and Operation of Water Resources Systems*, IAHS Press, Institute of Hydrology, Wallingford, Oxfordshire, UK

Beven, K. J., and Kirkby, M. J. (1979). "A physically-based variable contributing area model of basin hydrology." *Hydrol. Sci. Bull.*, 24(1), 43–69.

Birikundavyi, S., Labib, R., Trung, H. T. and Rousselle, J. (2002), "Perofrmance of Neural Networks in Daily Streamflow Forecasting", Journal of Hydrologic Engineering, ASCE, 7(5), 392-398.

Burnash, R. J. C., Ferral, R. L., and McGuire, R. A. (1973a). "A generalized streamflow simulation system—conceptual modeling for digital computers." *Rep.*, U.S. Dept. of Commerce, National Weather Service, Silver Springs, Md., and State of California, Dept. of Water Resources, Sacramento, Calif.

Burnash, R. J. C., Ferral, R. L., and McGuire, R. A. (1973a). "A generalized streamflow simulation system—conceptual modeling for digital computers." *Rep.*, U.S. Dept. of Commerce, National Weather Service, Silver Springs, Md., and State of California, Dept. of Water Resources, Sacramento, Calif.

Crawford, N. H., and Linsley, R. K. (1966). "Digital simulation in hydrology: Stanford Watershed Model IV." *Tech. Rep. No. 39*, Stanford Univ., Palo Alto, Calif.

Dawdy, D. R., and O'Donnell, T. (1965). "Mathematical models of catchment behavior." *J. Hydraul. Div., Am. Soc. Civ. Eng.*, 91(HY4), 123–127.

Deursen, W.P.A. van and J.C.J. Kwadijk, (1994). RHINEFLOW: an integrated GIS water balance model for the River Rhine. In: Kovar K. and H.P. Nachtnebel (eds) Application of Geographic Information Systems in Hydrology and Water Resources Management. Proceedings of the conference HYUROGIS '93. IHAS publicationno 211, pp 507-519. Wallingford: IHAS publications.

Duan, Q., Sorooshian, S., and Gupta, V. (1992). "Effective and efficient global optimisation for conceptual Rainfall-Runoff models." Water resources research., 28(4), 1015-1031.

Durand, P., Odoux C. G., and Cordier, M.O. (2002). "Parameterisation of hydrological models: a review and lessons learned form studies of an agricultural catchment (Naizin, France)." Agronomie., 22, 217-228.

Kwadijk, J.C.J., 1993. The impact of climate change on discharge of the River Rhine. PhD-thesis University of Utmcht, DepartmmntofPhysical Geography.

Lempert, M. (1993). "Die Bestimmung des oberflächenabflusses aus regionalisierten kenngrößen auf der Grundlage von Rasterflächen." Diplomarbeit, Geographisches Institut, Universtität Frieburg, Freiburg, Univeröffentlicht.

Leavesley, G. H., Lichty, R. W., Troutman, B. M., and Saindon, L. G. (1983). "Precipitation-runoff modeling system user's manual." *USGS Water Resources Investigations Rep. No. 83-4238*, Denver.

Madsen, H. (2003). "Parameter estimation in distributed hydrological catchment modelling using automatic calibration with multiple objectives." Advances in water resources., 26, 205-216.

Madsen, H. (2000). "Automatic calibration and uncertainty assessment in rainfall-runoff modelling, 2000 joint conference on water resources engineering and water resources planning and management." Hyatt Regency Minneapolis, USA, July 30 – August 2.

Metcalf and Eddy, Inc., Univ. of Florida, and Water Resources Engineers, Inc. (1971). "Storm water management model, Vol. 1—Final report." *EPA Rep. No. 11024DOC07/71 (NITS PB-203289)*, EPA, Washington, D.C.

Menzel, L. (1997). "Modellierung der Evapotranpiration im system Boden – Pflanze – Atmosphäre." Helft 67, Geographisches Institut ETH.

Mitas L. and Mitasoca H. (1998), Distributed soil erosion simulation for effective erosion prevention. *Water Resources Research* 34: 505 - 16

Morris, E. M. (1980). "Forecasting flood flows in grassy and forested basins using a deterministic distributed mathematical model." *IAHS Publication No. 129 (Hydrological Forecasting)*, International Association of Hydrological Sciences, Wallingford, U.K., 247–255.

Ostrowski, M., Lempert, M. and Heusch S. (2003). "A mathematical mdoel for the identification of human impacts on flood: the Modau case study." In: *Modelling in Natural sciences*, Müller, T., and Müller, H, eds., Springer, 335-356.

Rockwood, D. M. (1982). "Theory and practice of the SSARR model as related to analyzing and forecasting the response of hydrologic systems." *Applied modeling in catchment hydrology*, V. P. Singh, ed., Water Resources Publications, Littleton, Colo., 87–106.

Schot, P. P., Poot, A., Vonk, G. A., and Peeters, W.H.M. (2001). "A surface water model for the Orinoco river basin." Technical report. Utrecht.

Scurlock, J. M. O., Asner, G. P. and Gower, S. T. (2001). "Worldwide historical estimates of leaf area index 1932-2000." Oak Ridge national laboratory.

Schultz, G.A., 1988. Remote Sensing in Hydrology. *Journal of Hydrology*, vol. 100, pp. 239-265.

Singh, V. P. (1995). "Chapter 1: Watershed Modeling." *Computer models of watershed hydrology*." Water Resources Publications, Colorado.

Singh, V. P. (1992). "Chapter 8: Infiltration and Soil Moisture." *Elementary Hydrology. Prentice Hall,* 203-268.

Singh, V. P., Woolhiser, A. D. (2002). "Mathematical modelling of watershed hydrology", Journal of Hydrologic Engineering., 7(4), 270-284.

Smith, M., Allen, R., Monteith, J. L., Perrier, A., Santos Pereira, L. and Segeren, A. (1992). Expert consultation on revision of FAO methodologies for crop water requirements. Land and Water Development Division, Food and Agriculture Organization of the United Nations, Rome.

Sorooshian, S., and Gupta V. K. (1995). "Chapter 2: Model Calibration." *Computer models of watershed hydrology*, Water Resources Publications, Colorado.

Thomthwaite,C.W. and J.R. Mather, 1957. lnstmctions and tables for computing potential evapotmnspiration and the water balance. Publications in climatology X, pp 183-243.

Western, A. W., and Grayson, R. B. (2000). "Chapter 9: Soil moisture and runoff processes at Tarrawarra." *Spatial patterns in Catchment hydrology: Observations and Modelling*, Grayson, R. B. and Blöschl, eds., Cambridge university press, Cambridge.

Western, A. W., and Grayson, R. B. (1998). The Tarrawarra data set: Soil moisture patterns, Soil characteristics and Hydrological flux measurements. Water Resources Research, 34 (10), 2765-2768.

Wurbs, R. A. ~1998!. ''Dissemination of generalized water resources models in the United States.'' *Water Int.*, 23, 190–198.

Yapo, P.O., Gupta, V.H. and Sorooshian S. (1998), "Multi-objective global optimisation for hydrologic models." Journal of Hydrology., 204, 83-97.

Zhang, B. and Govindraju, S. (2000), "Prediction of Watershed Runoff using Bayesian Concepts and Modular Neural Networks." Water Resources Research, 36 (3), 753-762.

Zhang, Xiaohui, (1997) Integration of A Stochastic Space-time Rainfall Model and Distributed Hydrologic Simulation with GIS, Ph.D. Dissertation, University of Arizona, Tucson, AZ, USA.

Appendix – A

Discussion on leaf area index

LAI is a key parameter for global and regional models of biosphere/atmosphere exchange of carbon dioxide, water vapour and other materials. It also plays major role in determining the energy balance of the land surface. Methodologies for determining LAI have changed over the decades. It is useful to represent the inconsistencies that are actually found in the scientific literature.

LAI is broadly defined as the amount of leaf area in a vegetation canopy per unit land area. LAI is a key structural characteristic of vegetation and land cover because of the role of green leaves in a wide range of biological and physical processes. LAI may be described most simply as

$$LAI = \frac{S}{G}$$

Where S is the functional (green) leaf area of the canopy standing on ground area G.

Most commonly "S" is measured as the projected area. However, LAI may be more precisely defined in a number of different ways. For example, LAI may be measured as

the total surface area of leaves in a canopy. This will be equal to 2S for flat leaves and greater than 2S for needle shaped and succulent leaves and photosynthetic stems.

According to Barclay (1998), there are at least four common measures of LAI.

Def (1): Total LAI is based on the total outside area of the leaves, taking leaf shape into account, per unit area of horizontal land below the canopy.

Def (2): One-sided LAI is usually defined as half the total LAI, even if the two sides of the leaves are not symmetrical.

Def (3): Horizontally projected LAI is the area of "shadow" that would be cast by each leaf in the canopy with a light source at infinite distance and perpendicular to it, summed up for all leaves in the canopy.

Def (4): Inclined projected LAI represents the projected area of leaves taking into account individual leaf inclinations.

Def (1) is rarely used. Def (2) suffers from the problem that the meaning of "one sided" is unclear for coniferous needles, highly clumped foliage, or rolled leaves.. Chen and Black (1992) suggest that the LAI of non-flat leaves should be defined as half the total intercepting area per unit ground area, and that def (3) should be abandoned. In the recent literature, def (4) is being used.

Appendix B

Soil horizons

Most soils have a distinctive profile or sequence of horizontal layers. Generally, these horizons result from the soil processes of eluviation and organic activity. Five general layers are normally present in a typical soil: O, A, B, C, and R horizons (Figure A1).

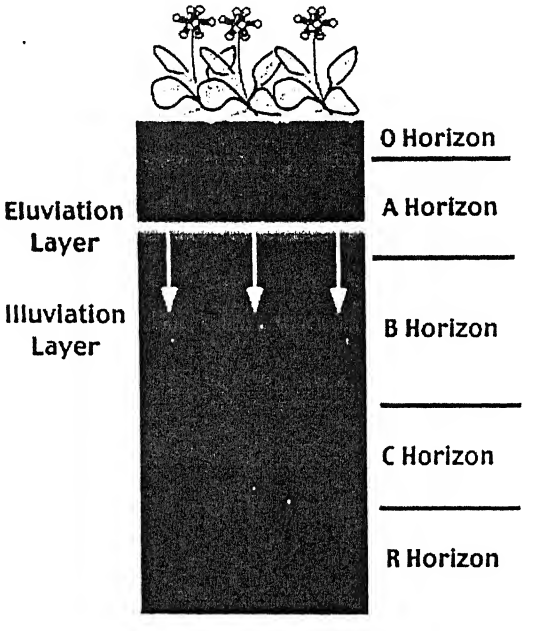

Figure A1: Typical layers found in a soil profile.

The O horizon is the topmost layer of most soils. It is composed mainly of plant litter at various levels of decomposition and humus. Below it is the A-horizon. This layer is composed primarily of mineral particles, which has two characteristics: it is the layer in

which humus and other organic materials are mixed with mineral particles, and it is a zone of translocation from which eluviation has removed finer particles and soluble substances, both of which may be deposited at a lower layer. Thus the A horizon is dark in color and usually light in texture and porous. The A horizon is commonly differentiated into a darker upper horizon or organic accumulation, and a lower horizon showing loss of material by eluviation.

The B horizon is a mineral soil layer which is dominated by illuviation. It receives material eluviated from the A horizon. This layer also has a higher bulk density than the A horizon due to its enrichment of clay particles. The B horizon may be colored by oxides of iron and aluminum or by calcium carbonate illuviated from the A horizon. These horizons can be divided into A1, A2 and A3 or B1, B2 and B3 starting from top.

The C horizon is composed of weathered parent material that has not been yet significantly affected by the pedogenic processes or translocation and organic modification.

The R horizon consists of unweathered bedrock.

Source: http://www.physicalgeography.net/fundamentals/10t.html